https://doi.org/10.5194/egusphere-2025-167
Preprint. Discussion started: 25 April 2025

Modeling organic aerosol over Central Europe: uncertainties linked to different chemical mechanisms, parameterizations, and boundary conditions

Lukáš Bartík[1], Peter Huszár[1], Jan Peiker[1], Jan Karlický[1], Ondřej Vlček[2], and Petr Vodička[3]

[1]Department of Atmospheric Physics, Faculty of Mathematics and Physics, Charles University, Prague, V Holešovičkách 2, 18000 Prague 8, Czech Republic
[2]Czech Hydrometeorological Institute, Na Šabatce 2050/17, 143 06 Prague 4, Czech Republic
[3]Institute of Chemical Process Fundamentals of the Czech Academy of Science, Rozvojová 1/135, 165 02, Prague 6, Czech Republic

Correspondence: Lukáš Bartík (lukas.bartik@matfyz.cuni.cz)

Abstract.

This study explores the uncertainties in modeling organic aerosol (OA) over Central Europe, focusing on the roles of chemical mechanisms, emission parameterizations, and boundary conditions. Organic aerosols, particularly secondary organic aerosols (SOAs), significantly influence climate, health, and visibility, comprising up to 90 % of submicron particulate matter. Using the Comprehensive Air Quality Model with Extensions (CAMx) coupled with the Weather Research and Forecast Model, sensitivity analyses were conducted to assess the impact of intermediate-volatility organic compounds (IVOCs), semi-volatile organic compounds (SVOCs), and chemical boundary conditions on primary and secondary organic aerosol concentrations.

Results showed that including source-specific IVOC and SVOC emissions significantly improved CAMx's performance in reproducing observed OA levels, mainly when using the 1.5-dimensional Volatility Basis Set framework with activated chemical aging. For example, the domain-averaged SOA concentrations increased by up to 1.17 $\mu g\,m^{-3}$ during summer when both IVOC and SVOC emissions were included. Furthermore, incorporating OA into the boundary conditions enhanced model predictions, with the accuracy of modeled organic carbon concentrations improving by up to 100 % during summer at some monitoring sites. Despite these improvements, challenges remain due to uncertainties in emission estimates, parameterization schemes, and the spatial resolution of the models.

The findings underscore the importance of refined parameterizations for IVOC and SVOC emissions, higher temporal and spatial resolution in chemical boundary conditions, and better representation of chemical aging. Addressing these gaps in future studies will further enhance the understanding and prediction of OA dynamics in regional air quality modeling.

1 Introduction

Atmospheric aerosols are liquid or solid particles suspended in the atmosphere, which have substantial climate impacts via direct and indirect radiative effects (Li et al., 2022; Arola et al., 2022), negatively affect human health (Arias-Pérez et al., 2020; Ain and Qamar, 2021), reduce visibility (Singh and Dey, 2012), and have an undoubted environmental footprint, especially

https://doi.org/10.5194/egusphere-2025-167
Preprint. Discussion started: 25 April 2025

near large urban areas (Wu and Boor, 2021). Organic aerosol (OA) constitutes a significant fraction of the total aerosol in the submicron range (PM_1; particles with an aerodynamic diameter less than 1 μm). In terms of the total mass of PM_1, OA can account for as much as 90 % (Jimenez et al., 2009; Zhang et al., 2011; Crippa et al., 2014; Chen et al., 2022). For instance, in Europe, Lanz et al. (2010) reported OA contributions to the total PM_1 mass ranging from 36 to 81 %, while Morgan et al. (2010) measured values between 20 and 50 %. Additionally, these contributions tend to be higher over urban areas compared to rural ones (Bressi et al., 2013; Sandrini et al., 2016). Recently, Chen et al. (2022) noted that oxygenated OA components, which serve as proxies for secondary organic aerosol (SOA), comprise between 43.7 and 100 % of the submicron OA mass in Europe. They also stated that solid fuel combustion-related OA components still represent a significant portion of the submicron OA mass, particularly during winter (on average 21.4 %). These experimental findings highlight the need to identify sources of OA and assess their contributions to total concentrations of OA. Only based on their knowledge is it possible to develop effective strategies for reducing overall OA concentrations. Chemical transport models (CTMs) are essential tools for achieving these goals.

Over the past two decades, the approaches utilized for OA modeling in CTMs have evolved considerably. Traditionally, the modeling of primary (directly emitted) organic aerosol (POA) in CTMs has assumed that POA is non-volatile and chemically inert. At the same time, SOA formation has typically been modeled using the gas–particle partitioning of condensable products originating from the oxidation of reactive organic gases (e.g., Strader et al., 1999; Schell et al., 2001; Byun and Schere, 2006). This partitioning has often been approximated by applying absorptive partitioning in a pseudo-ideal solution (Pankow, 1994; Odum et al., 1996). Contrary to the traditional assumptions about POA, the experimental results showed that POA is mostly semi-volatile under ambient conditions, and the gas-phase portion can undergo photochemical oxidation, resulting in SOA formation (e.g., Robinson et al., 2007; Donahue et al., 2009). These findings led Donahue and his colleagues to develop two unified frameworks for gas–particle partitioning and chemical aging of both POA and SOA, known as volatility basis sets (VBSs). The first of these frameworks, referred to as the 1-dimensional (1-D) VBS, describes the evolution of OA by employing a set of lumped semi-volatile OA species with their volatilities equally spaced in a logarithmic scale (the basis set) (Donahue et al., 2006). In terms of effective saturation concentrations ($C^\star$) at a thermodynamic temperature of 298 K, 1-D VBS typically range from 0.01 to 10^6 $\mu g\,m^{-3}$, which covers three subcategories of organic compounds: low volatility organic compounds (LVOCs; $C^\star = \{0.01, 0.1\}$ $\mu g\,m^{-3}$), semi-volatile organic compounds (SVOCs; $C^\star = \{1, 10, 100\}$ $\mu g\,m^{-3}$), and intermediate volatility organic compounds (IVOCs; $C^\star = \{10^3, 10^4, 10^5, 10^6\}$ $\mu g\,m^{-3}$) (Donahue et al., 2009). The second framework, known as the 2-dimensional (2-D) VBS, describes the evolution of OA in a 2-D space defined by volatility and the degree of oxidation (Donahue et al., 2011, 2012). Later, Koo et al. (2014) developed a 1.5-dimensional (1.5-D) VBS approach that is based on the 1-D VBS framework but accounts for changes in the oxidation state of OA as well as its volatility using multiple reaction trajectories defined in the 2-D space of the 2-D VBS framework. However, despite these advances in OA modeling, CTMs still face challenges in accurately reproducing measured OA concentrations, mainly due to the underestimation of SOA concentrations.

Several studies have shown that using both the original 1.5-D VBS and its various modifications, along with the inclusion of emission estimates for missing SOA precursors, can significantly improve the model predictions of SOA in different regions

https://doi.org/10.5194/egusphere-2025-167
Preprint. Discussion started: 25 April 2025

of the Earth (e.g., Zhang et al., 2023; Jiang et al., 2021, 2019b; Yao et al., 2020; Giani et al., 2019; Meroni et al., 2017; Ciarelli et al., 2017; Woody et al., 2016). The term “missing SOA precursors" means IVOCs and SVOCs, as they are missing in traditional emission inventories used to create input emission data for CTMs. However, these studies also indicate that the degree of improvement achieved is accompanied by considerable uncertainty. This uncertainty is partly caused by the inaccuracy of a large number of parameters characterizing individual basic sets, such as, for example, effective enthalpies of vaporization of POA and SOA species, product mass yields for oxidation of IVOCs, and the reaction rates associated with these oxidations, which are constrained using data obtained from smog chamber experiments. It was demonstrated, for example, by Jiang et al. (2021), who significantly improved the modeled concentrations of OA and SOA over Europe during winter by using optimized parameters in the basis sets for POA and SOA originating from biomass burning. These optimized parameters were specifically determined to account for the losses of semi-volatile vapors on the walls of the smog chamber used in the experiments conducted to determine them. Similarly, Ciarelli et al. (2017) updated a modified 1.5-D VBS scheme with parameters determined based on novel smog chamber experiments focused on biomass burning and showed that these updates significantly improved the modeled concentrations of total OA and SOA over Europe. Also, Jiang et al. (2019b) created a modified 1.5-D VBS scheme, optimized using parameters based on current smog chamber experiments focused on emissions from diesel cars and biomass burning. They demonstrated that this modified VBS scheme improved the model performance for total OA as well as its components, including hydrocarbon-like OA, biomass-burning-like OA, and oxygenated OA components.

Another significant source of uncertainty in the modeled concentrations of OA and its components when using traditional emission inventories are the emission estimates of missing SOA precursors and the volatility distribution factors for POA emissions. Regarding IVOC emissions, many previous works (e.g., Meroni et al., 2017; Denier van der Gon et al., 2015; Koo et al., 2014; Tsimpidi et al., 2010) estimated them using a source-non-specific parameterization (IVOC = 1.5 $\times$ POA) proposed by Robinson et al. (2007). However, this simplifying assumption has been partially addressed over time by establishing several source-specific parameterizations for IVOC emission estimates. These parameterizations were derived from smog chamber experiments conducted with emissions from various sources, such as biomass burning, diesel vehicles, and gasoline vehicles (e.g., Jiang et al., 2021; Giani et al., 2019; Ciarelli et al., 2017; Zhao et al., 2016, 2015; Jathar et al., 2014). Further, in order to account for missing SVOC emissions in model simulations employing VBS approaches, many researchers have opted to increase the amount of POA emissions by a factor of 3 (e.g., Jiang et al., 2021, 2019b; Li et al., 2020; Ciarelli et al., 2017, 2016; Matsui et al., 2014; Shrivastava et al., 2011; Hodzic et al., 2010; Tsimpidi et al., 2010). This adjustment is based on partition theory predictions to compensate for missing gaseous emissions in the semi-volatile range (Ciarelli et al., 2017) so that the adjusted POA emissions should represent total primary organic matter in the entire semi-volatile range (POM_{SV}). Here, it is appropriate to note that this approach is in good agreement with the results of Denier van der Gon et al. (2015), who constructed a revised European bottom-up emission inventory for residential wood combustion accounting for SVOCs and showed that the revised emissions are higher than those in the previous inventory by a factor of 2–3 but with substantial inter-country variation. Recently, to overcome the above-mentioned theory-based approach to estimating POM_{SV}, Giani et al. (2019) used the experimental studies of Zhao et al. (2015) and Zhao et al. (2016), which examined emissions from diesel and gasoline

https://doi.org/10.5194/egusphere-2025-167
Preprint. Discussion started: 25 April 2025

vehicles, respectively. These studies provided not only estimates of IVOC emissions, scaled according to emissions of non-methane hydrocarbons but also the complete volatility distributions of these emissions. Using these distributions, Giani et al. (2019) could determine the ratios between IVOC and POM_{SV} emissions. Subsequently, using these ratios, they determined the POM_{SV} emissions themselves.

In this study, we present two sensitivity analyses focused on various aspects related to the transport and chemistry of OA over Central Europe. The first analysis investigates how estimates of IVOC and POM_{SV} emissions influence the modeled concentrations of OA, considering various model approaches to gas-phase chemistry and the chemical and thermodynamic processes associated with OA. In comparison with previous works devoted to a similar topic over Europe (e.g., Jiang et al., 2021; Giani et al., 2019; Ciarelli et al., 2017; Meroni et al., 2017; Ciarelli et al., 2016), which focused mainly on the winter period, we concentrate on the winter and summer periods in our study. The second sensitivity analysis evaluates the impact of large-scale transport of OA, i.e., the effect of incorporating OA data, including their partition to primary and secondary fractions, into the chemical boundary conditions. Due to the size and location of the model domain we used, this type of sensitivity analysis is crucial.

2 Methodology

All model experiments utilized in this study were conducted using the Comprehensive Air Quality Model with Extensions (CAMx) version 7.10 (Ramboll, 2020), which was offline coupled with the Weather Research and Forecast (WRF) Model version 4.2 (Skamarock et al., 2019) and the Model of Emissions of Gases and Aerosols from Nature (MEGAN) version 2.10 (Guenther et al., 2012). The two model experiments employed in both sensitivity analyses (henceforth referred to as CSwI and CVb) were taken from the work of Bartík et al. (2024), in which they represent the base simulations of the SOAP and VBS experiments. All additional experiments were conducted on the same Central European model domain as CSwI and CVb. This domain, characterized by a horizontal resolution of 9 $\mathrm{km} \times 9\ \mathrm{km}$, is centered over Prague (50.075° N, 14.44° E), Czech Republic (Fig. 1). In addition, these additional experiments were carried out for the same period as CSwI and CVb (i.e., for the years 2018 and 2019) and utilized the same driving meteorological fields as these two experiments. A comprehensive description of the model domain and the configuration of the WRF model simulation used to produce the driving meteorological fields can be found in Bartík et al. (2024).

2.1 CAMx and its configurations used

CAMx is a state-of-the-art Eulerian CTM designed to simulate all key processes involved in the transport and chemistry of pollutants. These processes include horizontal and vertical advection, horizontal and vertical diffusion, gas-phase and aerosol chemistry, and wet and dry deposition.

To solve gas-phase chemistry in the model experiments, we used two different mechanisms. The first mechanism was the fifth revision of the Carbon Bond mechanism version 6 (CB6r5), which contains 233 reactions among 87 species (62 state gases and 25 radicals; Ramboll, 2020). The second mechanism was SAPRC07TC, the version of the Statewide Air Pollution

https://doi.org/10.5194/egusphere-2025-167
Preprint. Discussion started: 25 April 2025

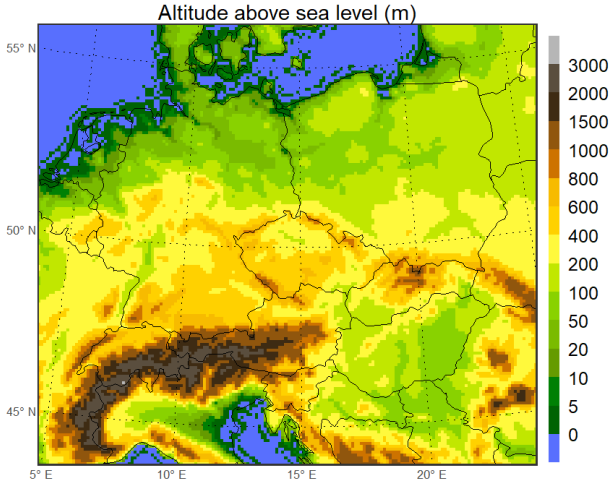

Figure 1. Resolved model terrain altitude above sea level (in m).

Research Center 2007 mechanism (Carter, 2010; Hutzell et al., 2012). SAPRC07TC includes 565 reactions among 117 species (72 state gases and 45 radicals; Ramboll, 2020). To solve both mechanisms numerically, we applied the Euler Backward Iterative method developed by Hertel et al. (1993).

Further, we employed a static two-mode coarse/fine (CF) scheme to run gas-phase chemistry with aerosol chemistry processes. This scheme divides the aerosol size distribution into two static modes (coarse and fine). To predict the composition and physical state of inorganic aerosols, we used the thermodynamic equilibrium model ISORROPIA version 1.7 (Nenes et al., 1998, 1999). Aqueous aerosol formation in resolved cloud water was calculated using the modified version of the RADM (Regional Acid Deposition Model) aqueous chemistry algorithm (Ramboll, 2020), developed initially by Chang et al. (1987). Among others, the RADM algorithm handles the aqueous formation of SOA from glyoxal, methyl glyoxal, and glycolaldehyde (Ortiz-Montalvo et al., 2012; Lim et al., 2013). Two modules are responsible for controlling organic gas–particle partitioning and oxidation chemistry in CAMx version 7.10 (Ramboll, 2020). The first is the Secondary Organic Aerosol Processor (SOAP) version 2.2, which was initially developed by Strader et al. (1999). The second module is 1.5-D VBS created by Koo et al. (2014). Since both modules are utilized in our model experiments, it is essential to clarify their differences, which we address in Appendix A.

Additionally, we used the CAMx wet deposition model (Ramboll, 2020) to solve the wet deposition of gases and aerosols. To calculate the dry deposition of gases and aerosols, we utilized the methods of Zhang et al. (2003) and Zhang et al. (2001), respectively.

2.2 Input emission data and chemical boundary conditions

The input emission data employed in the model experiments can be categorized into two groups. The first group comprises biogenic and traditional anthropogenic emissions, which remain consistent across all the model experiments except for POA

https://doi.org/10.5194/egusphere-2025-167
Preprint. Discussion started: 25 April 2025

emissions, as will be discussed later. A more comprehensive description of these emissions and their preparation for the model experiments can be found in Bartík et al. (2024). In summary, anthropogenic emissions outside the territory of the Czech Republic were sourced from the CAMS (Copernicus Atmosphere Monitoring Service) European anthropogenic emissions - Air Pollutants inventory version 4.2 (CAMS-REG-v4.2; Kuenen et al., 2021) for the year 2018. Within the Czech Republic, we utilized high-resolution emissions from the Register of Emissions and Air Pollution Sources (REZZO – Registr emisí a zdrojů znečištění ovzduší) for the year 2018, along with emissions from the ATEM Traffic Emissions dataset for the year 2016. The REZZO emissions were provided by the Czech Hydrometeorological Institute (https://www.chmi.cz), while the ATEM dataset was supplied by ATEM (Ateliér ekologických modelů – Studio of Ecological Models; https://www.atem.cz). The raw anthropogenic emissions were interpolated into the model grid and the temporal disaggregation and speciation were carried out using the FUME emission preprocessor (Benešová et al., 2018; Belda et al., 2024). BVOC emissions were calculated using MEGAN version 2.1 (Guenther et al., 2012).

The second group includes IVOC and SVOC emissions from anthropogenic sources. As these emissions are not part of the used emission inventories, we estimated them using sector-specific or sector-non-specific parameterizations, which will be discussed in greater detail in the subsequent subsection.

To force the model experiments at the boundary of the model domain, we employed two distinct sets of chemical boundary conditions (CBCs). The first set consists of time-space invariant concentrations of the chemical species outlined in Table S1 in the Supplement. Henceforth, we will refer to this set as the default CBCs. As indicated in Table S1, the number of chemical species utilized for the default CBCs varies slightly based on the chosen gas-phase mechanism, which is influenced by their differing formulations. The second set of CBCs, subsequently referred to as the EAC4 CBCs, was developed using the monthly averaged fields of the CAMS global reanalysis (EAC4) dataset (Inness et al., 2019). Specifically, we utilized the mean monthly concentrations of gas-phase and aerosol species listed in Table S2 of the Supplement. This table also details the mapping used to convert the aerosol species from the EAC4 dataset to those recognized by the CF scheme. It is essential to emphasize that the inclusion of both hydrophobic and hydrophilic organic matter in the EAC4 dataset is crucial for the second sensitivity analysis. The methods for mapping these aerosol species to the OA species recognized by the CF scheme are explained in the following subsection.

2.3 Sensitivity analyses

2.3.1 First sensitivity analysis

As we mentioned in the introduction, the aim of the first sensitivity analysis is to examine how estimates of IVOC and POM_{SV} emissions influence the modeled concentrations of OA, considering various model approaches to gas-phase chemistry and the chemical and thermodynamic processes associated with OA. To achieve the objective of this sensitivity analysis, we utilized CSwI and CVb and developed four additional experiments, which include CSnI, SSnI, SSwI, and CVa (Table 1). These experiments can be split into two groups based on the module used to model OA chemistry.

https://doi.org/10.5194/egusphere-2025-167
Preprint. Discussion started: 25 April 2025

Table 1. Model setup (gas-phase chemistry mechanism, OA chemistry module, and additional aging) and the inclusion of IVOC and SVOC emission estimates in the individual experiments of the first sensitivity analysis. Notes: [a] The additional aging refers to the aging of SOA originating from biomass burning and biogenic sources, which is disabled by default in the 1.5-D VBS scheme.

Experiment	Gas-phase chemistry mechanism	OA chemistry module	Addiotional aging[a]	IVOC emission estimates included	SVOC emission estimates included
CSnI	CB6r5	SOAP	No	No	No
CSwI	CB6r5	SOAP	No	Yes	No
SSnI	SAPRC07TC	SOAP	No	No	No
SSwI	SAPRC07TC	SOAP	No	Yes	No
CVb	CB6r5	1.5-D VBS	No	Yes	Yes
CVa	CB6r5	1.5-D VBS	Yes	Yes	Yes

The first group comprises CSnI, CSwI, SSnI, and SSwI, all utilizing SOAP. At the same time, CB6r5 was applied to model gas-phase chemistry in CSnI and CSwI, while SAPRC07TC was used for this purpose in SSnI and SSwI. As for IVOC emissions, both CSwI and SSwI considered them, whereas CSnI and SSnI were conducted without their inclusion. The second group includes CVb and CVa, in which OA chemistry was modeled using the 1.5-D VBS scheme, the gas-phase chemistry was modeled using CB6r5, and the identical emission estimates of both IVOC and POM_{SV} were employed. The only difference between these two experiments lies in the consideration of the chemical aging of SOA originating from both biogenic emissions and biomass burning. While CVb did not account for this aging, it was activated in CVa, assuming a reaction rate of 2×10^{-11} $cm^3\,molecule^{-1}\,s^{-1}$ for these SOAs with hydroxyl radicals in the gas phase. This reaction rate corresponds with that used for the chemical aging of anthropogenic SOA (Appendix A).

Regarding the IVOC and POM_{SV} emission estimates used in individual experiments, Table 2 summarizes all the parameterizations applied to calculate them for the respective anthropogenic sources. It is important to note that in all four experiments utilizing SOAP, we applied POA emissions obtained from the traditional emission databases mentioned earlier. Given that these POA emissions come from traditional emission inventories, we assumed that they do not account for SVOCs. Therefore, in both experiments utilizing the 1.5-D VBS scheme, we replaced these POA emission estimates with those for POM_{SV}, which include missing SVOCs.

As can be seen in Table 2, we employed the exact IVOC emission estimates in SSwI as those used by Bartík et al. (2024) in CSwI. Furthermore, in CVa, we applied the identical IVOC and POM_{SV} emission estimates used by Bartík et al. (2024) in CVb, as previously noted. At the end of this subsection, it is essential to mention that all the experiments detailed here were realized using the default chemical boundary conditions and thus without considering any aerosols outside the model domain.

https://doi.org/10.5194/egusphere-2025-167
Preprint. Discussion started: 25 April 2025

Table 2. Parameterizations of the IVOC and POM_{SV} emission estimates used in the individual experiments of the first sensitivity analysis. The individual parameterizations were taken from [a] Giani et al. (2019), [b] Jiang et al. (2021), [c] Robinson et al. (2007). NMVOC stands for non-methane volatile compounds.

Experiment	Parameterization for	Gasoline vehicles (GV)	Diesel vehicles (DV)	Biomass burning (BB)	Other sources (OS)
CSnI	IVOC	0	0	0	0
CSwI	IVOC	$0.0397 \times NMVOC_{GV}$ [a]	$1.2748 \times NMVOC_{DV}$ [a]	$4.5 \times POA_{BB}$ [b]	$1.5 \times POA_{OS}$ [c]
SSnI	IVOC	0	0	0	0
SSwI	IVOC	$0.0397 \times NMVOC_{GV}$ [a]	$1.2748 \times NMVOC_{DV}$ [a]	$4.5 \times POA_{BB}$ [b]	$1.5 \times POA_{OS}$ [c]
CVb	IVOC	$0.0397 \times NMVOC_{GV}$ [a]	$1.2748 \times NMVOC_{DV}$ [a]	$4.5 \times POA_{BB}$ [b]	$1.5 \times POA_{OS}$ [c]
	POM_{SV}	$IVOC_{GV} / 4.62$ [a]	$IVOC_{DV} / 2.54$ [a]	$3 \times POA_{BB}$ [b]	$3 \times POA_{OS}$ [b]
CVa	IVOC	$0.0397 \times NMVOC_{GV}$ [a]	$1.2748 \times NMVOC_{DV}$ [a]	$4.5 \times POA_{BB}$ [b]	$1.5 \times POA_{OS}$ [c]
	POM_{SV}	$IVOC_{GV} / 4.62$ [a]	$IVOC_{DV} / 2.54$ [a]	$3 \times POA_{BB}$ [b]	$3 \times POA_{OS}$ [b]

2.3.2 Second sensitivity analysis

In order to study how the inclusion of OA in the chemical boundary conditions affects its concentrations inside the model domain, we established CSwI and CVb as two reference experiments since no aerosols were included in their CBCs. Following this, we conducted three sensitivity experiments for each of the reference experiments, namely Sp0s100, Sp50s50, and Sp100s0 for CSwI and Vp0s100, Vp50s50, and Vp100s0 for CVb. Each of these sensitivity experiments was performed using the same model setup and IVOC and POM_{SV} parameterizations as in its corresponding reference experiment, except for the chemical boundary conditions. In these sensitivity experiments, we used three modifications of the EAC4 CBCs, each differing in the proportions of POA and SOA within the total OA (Table 3).

We opted for this approach due to the uncertainties involved in mapping OA from the EAC4 dataset to the OA species recognized by the CF scheme. This mapping was necessary because while the EAC4 dataset provides OA concentrations categorized into hydrophobic and hydrophilic components, the CF scheme utilizes POA and SOA surrogate species (Table S2 in the Supplement). However, since the proportions of POA and SOA in both hydrophobic and hydrophilic OAs were unknown, we decided to merge both species into the total OA. Next, we considered three scenarios for redistributing the total OA between POA and SOA. The first two scenarios represented extreme cases: in the first scenario, we treated the total OA as entirely composed of POA, while in the second scenario, we treated it as consisting wholly of SOA. The third scenario assumed a 50 percent share of both POA and SOA. Subsequently, we used these scenarios to obtain three pairs of boundary conditions for POA and SOA. We then added the same boundary conditions for the remaining remapped aerosol species to each pair of these boundary conditions, yielding the three modifications of the EAC4 CBCs mentioned above. As we have indicated in Table 3, the modification prepared using the first scenario was used in Sp100s0 and Vp100s0, the modification

https://doi.org/10.5194/egusphere-2025-167
Preprint. Discussion started: 25 April 2025

Table 3. Percentage share of POA and SOA in the total OA at the boundary of the model domain in the individual experiments of the second sensitivity analysis.

Experiment	POA	SOA
CSwI	0 %	0 %
Sp0s100	0 %	100 %
Sp50s50	50 %	50 %
Sp100s0	100 %	0 %
CVb	0 %	0 %
Vp0s100	0 %	100 %
Vp50s50	50 %	50 %
Vp100s0	100 %	0 %

prepared using the second scenario was used in Sp0s100 and Vp0s100, and the modification prepared using the third scenario was used in Sp50s50 and Vp50s50.

Another challenge we encountered was determining how to redistribute POA and SOA within the EAC4 CBC modifications to their respective surrogate species utilized in both SOAP and the 1.5-D VBS scheme. To address this issue, we established two simplifying assumptions regarding the shares of the surrogate species in POA and SOA at the boundary of the model domain. First, we assumed that these shares are spatially invariant and only change seasonally. Second, we set the seasonal shares of the individual surrogate species in SOA at the boundary of the model domain equal to the domain-averaged mean seasonal shares of the corresponding surrogate species' concentrations to SOA concentration in the reference experiments, and we proceeded analogously for the surrogate species of POA. Subsequently, we used these seasonal shares as factors to redistribute POA and SOA within all three modifications of boundary conditions. Table S3 in the Supplement shows the factors utilized to redistribute SOA to the surrogate species used in SOAP. Tables S4 and S5 in the Supplement offer the factors employed to redistribute POA and SOA to their surrogate species used in the 1.5-D VBS scheme.

2.4 Validation

We conducted a detailed validation of both CSwI and CVb in our previous study (Bartík et al., 2024). This validation included an assessment of modeled predictions against measurements for fine particulate matter ($PM_{2.5}$) and its components (ammonium, nitrates, sulfates, elemental carbon, and organic carbon), nitrogen dioxide, and sulfur dioxide. Consequently, our focus here was solely on evaluating the modeled OA concentrations within the individual model experiments of both sensitivity studies. For this evaluation, we utilized organic carbon (OC) measurements collected at stations in the Czech Republic (Table S6 in the Supplement), which covered at least part of the modeled period of 2018 and 2019. Some of these measurements were obtained during two specific measuring campaigns, while the remainder were collected at the Prague–Suchdol and Košetice stations.

https://doi.org/10.5194/egusphere-2025-167
Preprint. Discussion started: 25 April 2025

The first campaign was conducted at the Kosmos, Ropice, and Vrchy stations in the northeastern part of the Czech Republic, specifically in the Třinecko area (Seibert et al., 2020). The second campaign took place at the Švermov, Libušín, and Zbečno stations, located in Central Bohemia, specifically within the Kladensko area (Seibert et al., 2021). Both campaigns were divided into winter and summer phases, the schedules of which can be found in Table S6 in the Supplement. During both campaigns, individual OC samples were continuously collected over 12 hours using sampling streams and collection heads to ensure representative sampling of the $PM_{2.5}$ fraction. Subsequently, the mean 12-hour OC concentrations were determined from the collected samples. For validation purposes, we further derived mean daily OC concentrations from the mean 12-hour OC concentrations. Concurrently, air temperature, wind speed, and relative humidity were measured at the sampling stations, allowing us to determine their mean daily values and validate these meteorological variables as well. The data from both campaigns were provided by the Czech Hydrometeorological Institute (https://www.chmi.cz).

The collection of PM_{10} (particulate matter with a diameter $\leq$ 10 μm) samples at the Prague–Suchdol station took place every fourth day for 24 h from 2 January to 30 May 2018. The samples were collected on prebaked (3 h, 800 °C) quartz fiber filters (Tissuequartz, Pall, 47 mm) using a Leckel sampler (Leckel GmbH, Germany). The filter cuts were analyzed for OC concentrations by a thermal-optical carbon analyzer (Sunset Laboratory Inc., USA) using the shortened EUSAAR2 protocol (Cavalli et al., 2010). The resulting mean daily OC concentrations were corrected to blank.

The measurements of OC at the Košetice station in the Vysočina Region during the modeled period were obtained from the EBAS database (https://ebas-data.nilu.no/default.aspx). These measurements represent OC within the $PM_{2.5}$ fraction and were taken at 4-hour intervals. For validation purposes, we derived mean daily OC concentrations from them.

In order to validate the modeled air temperature, wind speed, and air humidity for these two stations, the Czech Hydrometeorological Institute provided us with measurements of the mentioned quantities directly from the Košetice station and the Prague–Kbely station. We chose the Prague–Kbely station as a representative site for the Prague–Suchdol station, where meteorological variables were not directly measured.

The modeled mean daily OC concentrations were compared with their corresponding measured values using several statistical measures, including the mean bias (MB), root mean square error (RMSE), normalized mean square error (NMSE), index of agreement (IOA), and fraction of predictions within a factor of two of observations (FAC2). The definitions of these statistical measures can be found in Eq. (S1)–(S5) in the Supplement. In order to assess the modeled and measured mean daily air temperatures, wind speeds, and relative humidities, we employed MB, RMSE, NMSE, and IOA. For this assessment, we exclusively used the mean daily values of the mentioned meteorological variables from the days when the OC measurements were carried out.

3 Results and discussion

3.1 Validation of meteorological variables

Figure S1 in the Supplement compares the observed and modeled mean daily temperatures, wind speeds, and relative humidities at the Prague–Kbely and Košetice stations across the individual seasons. Figure S2 in the Supplement provides similar

https://doi.org/10.5194/egusphere-2025-167
Preprint. Discussion started: 25 April 2025

comparisons at the stations utilized in both campaigns during their winter and summer phases. Our focus here is on the differences between the modeled and observed daily means of these meteorological variables. Figure 2 depicts these differences at the Prague–Kbely and Košetice stations throughout the respective seasons. Figure 3 illustrates these differences at the stations involved in both campaigns during their winter and summer phases. Additionally, Table S7 in the Supplement summarizes the statistical comparison of the modeled and observed daily means of these meteorological variables at all the stations.

The WRF model generally tends to slightly underestimate the mean daily temperatures, typically up to 1.5 K (Figs. 2a, b and 3a–d). An exception to this trend is observed at the Prague–Kbely station, where the model slightly overestimates the mean daily temperatures (Fig. 2b). The maximum differences in the mean daily temperatures only exceptionally exceeded 4 K (Fig. 3d). The NMSEs for the mean daily temperatures reached the lowest values (mainly below 5×10^{-3} %) among all the NMSEs evaluated. At the same time, the IOAs for the mean daily temperatures achieved the highest values (mostly above 0.9) among all the IOAs assessed.

Regarding the mean daily wind speeds, the model typically tends to overestimate them more or less (Figs.2c, d and 3e–h), except for the Prague–Kbely station (Fig. 2d). At the Prague–Kbely and Košetice stations, the model showed a reasonable accuracy of their predictions in all the seasons, with IOAs exceeding 0.85 and NMSEs mostly below 10 %. In contrast, at the stations involved in both campaigns, the model overestimated them during both phases (MB = 3.2–4.3 $\mathrm{m\,s^{-1}}$ in the winter phases and MB = 1.1–2.2 $\mathrm{m\,s^{-1}}$ in the summer phases). At the same time, IOAs ranged from 0.1 to 0.54 and NMSEs between 29 % and 1320 %.

Figures 2e, f and 3i–l demonstrate that the model somewhat underestimates the mean daily relative humidities at most of the stations, usually up to 9.5 %. At the same time, the maximum differences in the daily relative humidities only sporadically

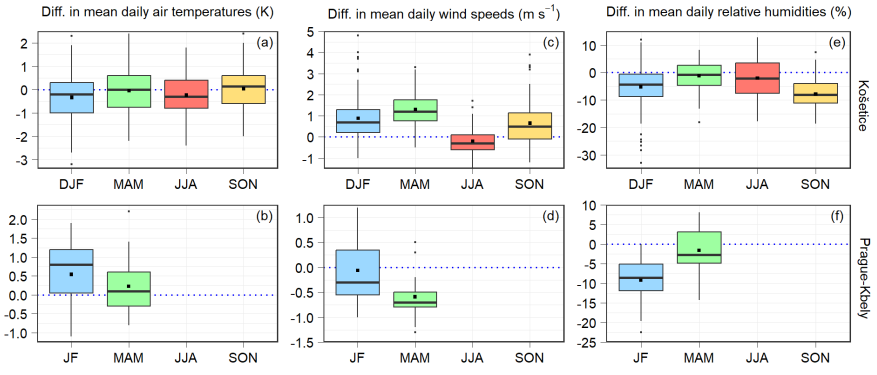

Figure 2. Differences between the modeled and observed mean daily air temperatures (in K) **(a, b)**, wind speeds (in $\mathrm{m\,s^{-1}}$) **(c, d)**, and relative humidities (in %) **(e, f)** at the Košetice station **(a, c, e)** during the winter (DJF), spring (MAM), summer (JJA), and autumn (SON) seasons of 2018 and 2019 and at the Prague–Kbely station **(b, d, f)** during January and February (JF) 2018 and the spring of 2018. The differences are shown in the form of box plots, the components of which are described in Fig. S3 in the Supplement. Blue dotted lines indicate the levels of zero differences.

https://doi.org/10.5194/egusphere-2025-167
Preprint. Discussion started: 25 April 2025

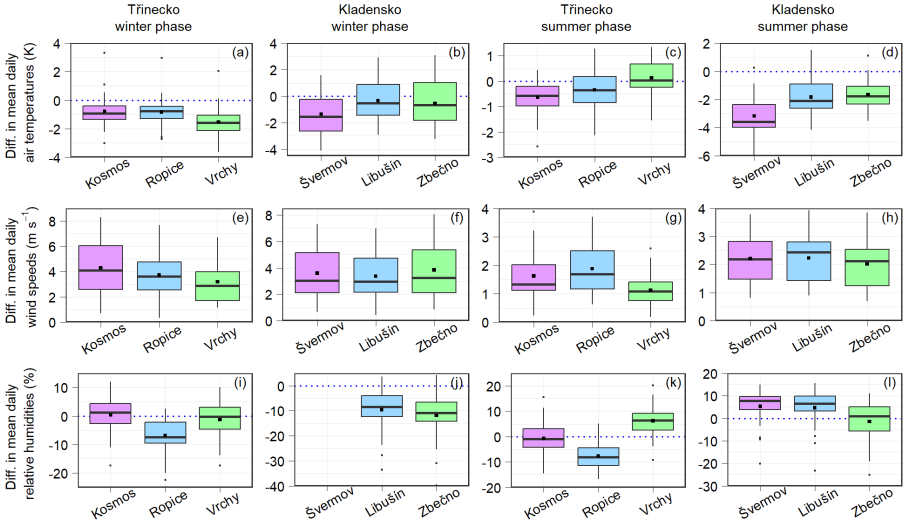

Figure 3. Differences between the modeled and observed mean daily air temperatures (in K) **(a–d)**, wind speeds (in m s^{-1}) **(e–h)**, and relative humidities (in %) **(i–j)** at the Kosmos, Ropice, and Vrchy stations in the Třinecko area during the winter **(a, e, i)** and summer **(c, g, k)** phase of the campaign and at the Švermov, Libušín, and Zbečno stations in the Kladensko area during the winter **(b, f, j)** and summer **(d, h, l)** phase of the campaign.

exceeded 20 %. The IOAs for the mean daily relative humidities exceeded 0.7 at most of the stations, while the NMSEs ranged between 0.5 % and 3.6%.

The overestimation of wind speed by the WRF model over the Central European domain with the same or similar horizontal resolution that we employed, especially in the winter months, was also pointed out in several papers (Huszar et al., 2020; Karlický et al., 2020; Liaskoni et al., 2023; Bartík et al., 2024). This overestimation could be one of the sources of underestimating OA concentrations in all the experiments analyzed here. Aksoyoglu et al. (2011) showed that the reduced modeled wind speeds during observed periods of low wind can increase $PM_{2.5}$ concentrations by a factor of 2–3. Since OA usually forms a significant part of $PM_{2.5}$, it can be assumed that similar increases also occur in OA concentrations under the mentioned conditions.

To further clarify the possible causes of the more substantial model overestimation of the mean daily wind speeds at the stations in the Kladensko area (Figs. 3f, h and S2f, h), we compared both the modeled and observed values of these wind speeds at the three stations with the corresponding wind speeds measured at four professional meteorological stations in Prague in Fig. S4. As can be seen, the modeled wind speeds at the stations in the Kladensko area are more accurately represented by the Prague stations, located approximately 15–45 km away, than by the local stations themselves. This finding suggests that the campaign's stations were placed in locations where the wind field was more substantially influenced by nearby obstacles, such as buildings and trees, and/or by the contours of the surrounding terrain. These same factors likely contributed to the more

https://doi.org/10.5194/egusphere-2025-167
Preprint. Discussion started: 25 April 2025

notable model overestimation of the mean daily wind speeds at some of the stations in the Třinecko area (Figs. 3e, g and S2e, g).

3.2 Sensitivity on SOA module and IVOC/POM$_{SV}$ emissions

In this subsection, we present and discuss the spatial distributions of the mean seasonal impacts on the concentrations of POA and SOA in the individual experiments of the first sensitivity analysis. Specifically, we focus on these impacts during the winters and summers of 2018–2019. We define these impacts in a specific experiment by the differences between the mean seasonal concentrations in this experiment and their corresponding values in the reference experiment. Before analyzing the mean seasonal impacts on the concentrations of a specific OA, we first outline the spatial distributions of the mean seasonal concentrations of this OA in the reference experiment. For this sensitivity study, we selected CSnI as the reference experiment since it was conducted without any additional emissions of IVOCs and SVOCs. Following this, we evaluate the organic carbon (OC) concentrations obtained from the individual experiments of this sensitivity analysis.

3.2.1 Spatial distributions of POA and SOA

The spatial distributions of the mean seasonal POA concentrations in the reference experiment during the winters and summers are depicted in Figs. 4a and b, respectively. The mean winter POA concentrations usually range between 0.1–9 $\mu g\,m^{-3}$, with the highest values reaching in the Po Valley (Italy) and some areas of the Czech Republic and Poland. In contrast, the mean summer POA concentrations mostly reach up to 0.3–0.5 $\mu g\,m^{-3}$, except for the area of the Po Valley, where they reach up to 1.5 $\mu g\,m^{-3}$.

Regarding the mean seasonal impacts on POA concentrations, Figs. 4c and d show their spatial distributions during the winters and summers, respectively. Additionally, the values of the domain-averaged mean seasonal impacts on POA concentrations are provided in Table S8 in the Supplement. The distributions of the mean seasonal POA concentrations in CSwI, SSnI, and SSwI are practically identical to those in CSnI in both seasons, leading to the negligible mean seasonal impacts on POA concentrations in these experiments. However, this is an expected result since the same POA emissions were used in all these experiments, and POA is not affected by the choice of gas-phase mechanisms and the addition of IVOC emissions when using SOAP. On the other hand, the addition of the SVOC emissions in CVb and CVa causes an increase in the mean seasonal POA concentrations over the entire domain in both seasons, resulting in positive mean seasonal impacts. The spatial distributions of the mean seasonal impacts in both experiments are similar to the mean seasonal POA concentrations in CSnI during both seasons. These similarities result from the scaling of SVOC emissions using both POA for most anthropogenic sources and NMVOC emissions for diesel and gasoline vehicles, which have similar spatial distributions to POA emissions from both types of vehicles. The most significant impacts in both experiments are observed in the Po Valley during both seasons, with the mean winter impacts reaching up to 10 $\mu g\,m^{-3}$ and the mean summer impacts reaching up to 1 $\mu g\,m^{-3}$. The comparison of the domain-averaged seasonal impacts in these two experiments shows that the mean seasonal POA concentrations increase on average across the entire domain in CVa by 0.02 $\mu g\,m^{-3}$ in both seasons. This observed increase could be attributed to the fact

https://doi.org/10.5194/egusphere-2025-167
Preprint. Discussion started: 25 April 2025

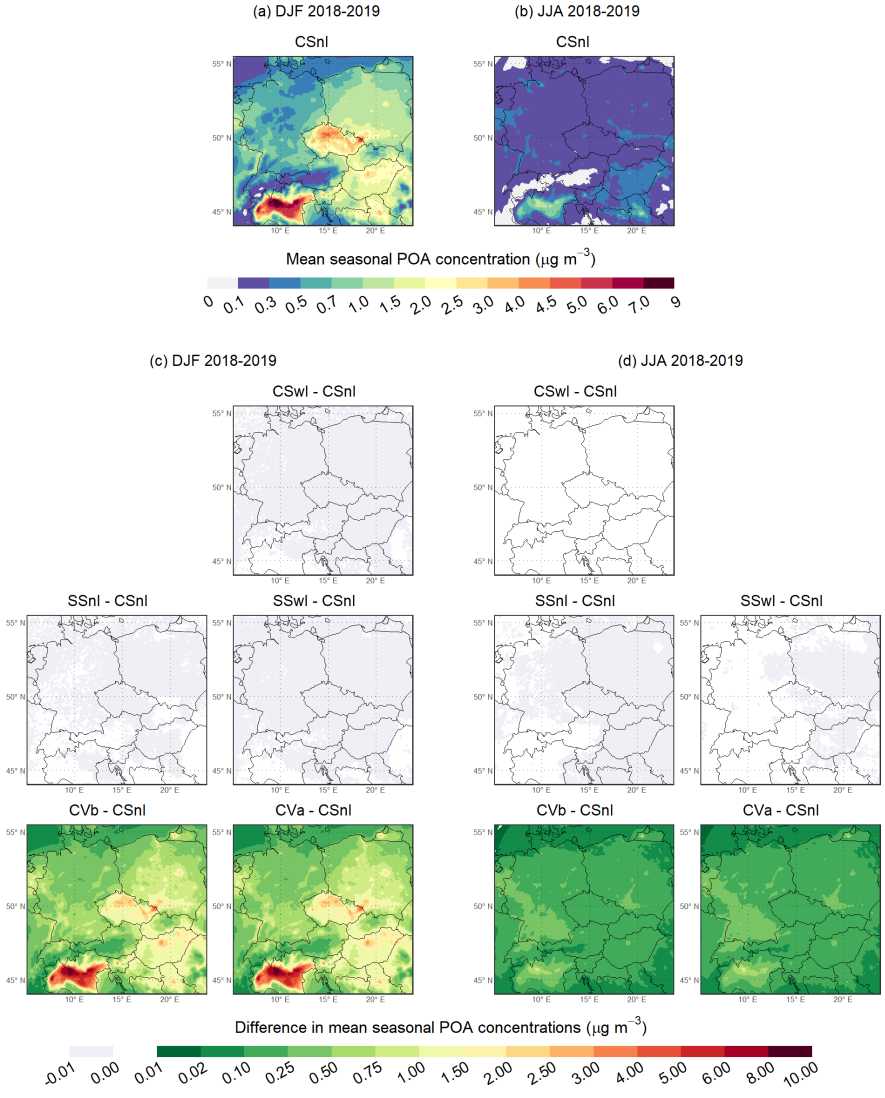

Figure 4. Mean seasonal POA concentration (in $\mu g\,m^{-3}$) in the reference experiment of the first sensitivity analysis (CSnI) during the winter **(a)** and summer **(b)** seasons of 2018 and 2019. The difference between the mean seasonal POA concentration predicted in the individual experiments of the first sensitivity analysis and its counterpart in the CSnI experiment (in $\mu g\,m^{-3}$) during the winter **(c)** and summer **(d)** seasons of 2018 and 2019.

that the additional aging of SOA gradually contributes to higher concentrations of the total OA, which subsequently shifts the thermodynamic equilibrium in the redistribution of POM_{SV} between the gas and aerosol phase toward the aerosol phase.

Figures 5a and b illustrate the spatial distributions of the mean seasonal SOA concentrations in the reference experiment during the winters and summers, respectively. The mean winter SOA concentrations in most of the territory of the domain

https://doi.org/10.5194/egusphere-2025-167
Preprint. Discussion started: 25 April 2025

reach up to 0.2–0.3 $\mu g\,m^{-3}$. In contrast, the mean summer SOA concentrations range between 0.6–1.6 $\mu g\,m^{-3}$ over most of
340 the domain, with the highest values occurring in the southern areas of the Pannonian Basin and southern Germany.

As for the mean seasonal impacts on SOA concentrations, Figs. 5c and d show their spatial distributions during the winters and summers, respectively. Furthermore, Table S8 includes the values of the domain-averaged mean seasonal impacts on SOA concentrations (ΔSOA). The distributions of the mean seasonal impacts in SSnI indicate that changing the mechanisms of gas-phase chemistry is almost not reflected in the mean winter SOA concentrations except for the central area of the Po Valley

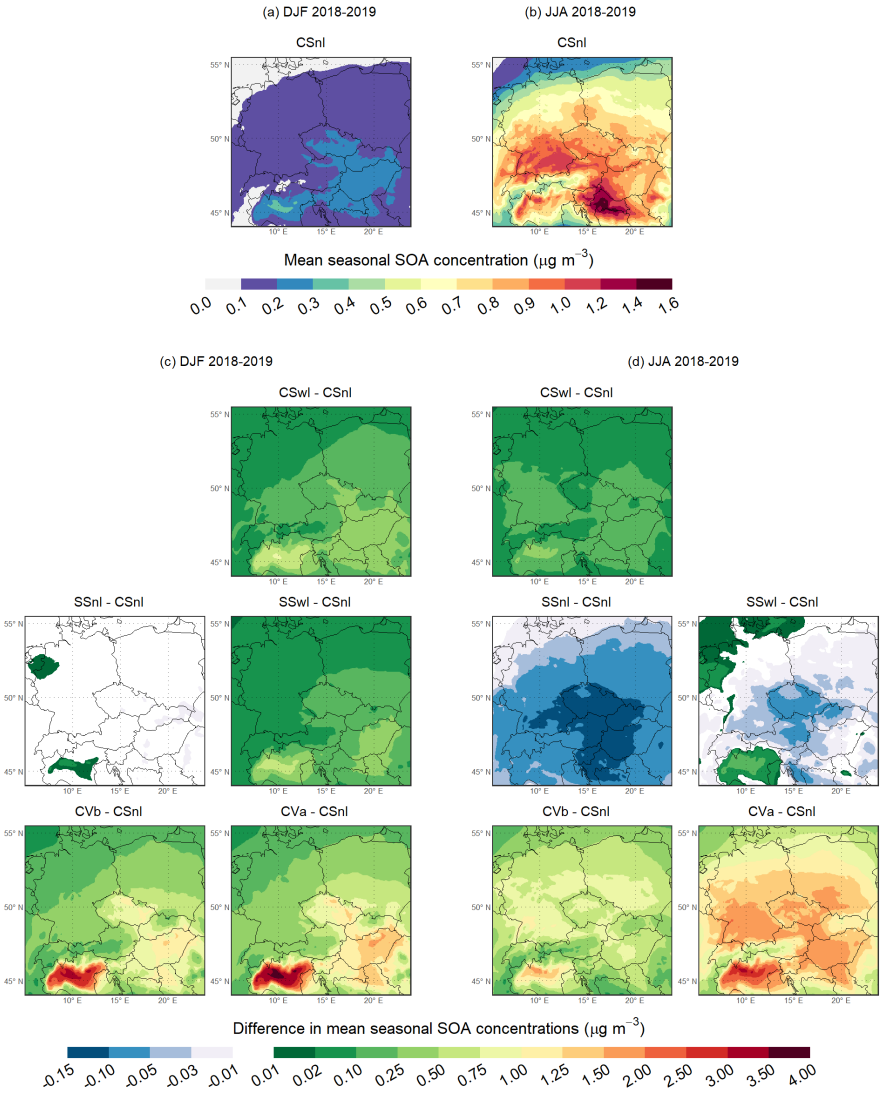

Figure 5. Same as Fig. 4 but for SOA.

https://doi.org/10.5194/egusphere-2025-167
Preprint. Discussion started: 25 April 2025

(ΔSOA = 0 $\mu g\,m^{-3}$), while it causes a decrease in the mean summer SOA concentrations in most areas of the domain by 0.1–0.15 $\mu g\,m^{-3}$ (ΔSOA = -0.07 $\mu g\,m^{-3}$). The addition of the IVOC emissions in CSwI and SSwI is manifested by the positive mean winter impacts over the entire domain, which are somewhat more pronounced in CSwI (ΔSOA = 0.17 $\mu g\,m^{-3}$) than in SSwI (ΔSOA = 0.12 $\mu g\,m^{-3}$). On the other hand, even adding the IVOC emissions in SSwI during the summer seasons does not cause positive mean seasonal impacts over the whole domain (ΔSOA = -0.01 $\mu g\,m^{-3}$), which is not the case in CSwI (ΔSOA = 0.09 $\mu g\,m^{-3}$). The simultaneous addition of the IVOC and SVOC emissions in CVb leads to a further increase in the mean seasonal impacts during both the winters (ΔSOA = 0.49 $\mu g\,m^{-3}$) and the summers (ΔSOA = 0.58 $\mu g\,m^{-3}$). Moreover, the additional aging of SOA in CVa raises the mean seasonal impacts even more during the winters (ΔSOA = 0.62 $\mu g\,m^{-3}$) and especially in the summers (ΔSOA = 1.17 $\mu g\,m^{-3}$), resulting in the highest overall seasonal impacts among all the experiments examined in this sensitivity analysis. During the winters, the areas with the greater impacts in CVa include the Czech Republic and the Pannonian Basin, where the impacts reach 0.75–2 $\mu g\,m^{-3}$. The highest impacts, reaching up to 4 $\mu g\,m^{-3}$, occur in the Po Valley. During the summers, the areas with the higher impacts include the Czech Republic, southern Germany and Poland, northern Austria, and the Pannonian Basin, where they reach 1.25–2.5 $\mu g\,m^{-3}$. Again, the Po Valley experiences the highest impacts, with values reaching up to 3.5 $\mu g\,m^{-3}$.

Several recent studies have been devoted to modeling the influence of IVOC and SVOC emissions on OA concentrations over Central Europe using the CAMx model. Meroni et al. (2017) modeled OA in the Po Valley area on a domain with a horizontal resolution of 5 $km \times 5$ km for the period of February 2013, and in one of the experiments, he used SOAP to control OA chemistry. Taking into account the differences in the emission inventories, spatial resolution, and period, the distribution of the mean monthly POA concentration in this experiment is qualitatively and quantitatively similar to the distribution of the mean seasonal POA concentration in CSwI. In contrast, the mean monthly SOA concentrations modeled by them, reaching a maximum of 0.3 $\mu g\,m^{-3}$, are smaller than the mean seasonal SOA concentrations in CSwI. This discrepancy may stem, in part, from their estimate of IVOC from all emission sectors as 1.5 $\times$ POA, based on the parameterization proposed by Robinson et al. (2007). For instance, IVOC emissions from biomass burning, which dominate total IVOC emissions during winter, were presumably significantly underestimated in their experiment compared to our estimate of these emissions (4.5 $\times$ POA).

Ciarelli et al. (2017) used a modified version of the 1.5-D VBS scheme to model OA over the European domain with a horizontal resolution of $0.25° \times 0.25°$ for the period between 25 February and 26 March 2009. To estimate the emissions of IVOCs and POM_{SV}, they used parameterizations that align closely with those used in CVa. When considering the same aspects as in the previous comparison, it is evident that the modeled distributions of the mean concentrations of POA and SOA in their experiment show qualitative similarities to the mean winter concentrations of POA and SOA observed in CVa. The main quantitative differences between the distributions of the mean POA concentrations could be attributed to the use of different emission inventories. It is important to emphasize here that our assumption about not including SVOC emissions in the emission inventories is only partially accurate. As noted by Kuenen et al. (2022), $PM_{2.5}$ emissions from small residential combustion, as reported in CAMS-REG-v4.2, include SVOC emissions for specific European countries. Italy is one such country, which suggests that the POM_{SV} estimates provided in CVb and CVa likely led to an overestimation of POA over its territory. This overestimation, in turn, has naturally influenced (increased) SOA levels in this region, especially during the winter months.

https://doi.org/10.5194/egusphere-2025-167
Preprint. Discussion started: 25 April 2025

However, it is crucial to note that CAMS-REG-v4.2 does not account for SVOC emissions from Central European countries, just as REZZO does not include them for the Czech Republic, thus justifying the use of POM_{SV} estimates in CVb and CVa.

Jiang et al. (2021) modeled OA over the European domain with a horizontal resolution of $0.25° \times 0.125°$ for the year 2011. Among the five experiments they performed, the SOAP and VBS_3POA experiments are the most similar to CSwI and CVb, respectively, in terms of setting the OA chemistry module and the IVOC and POM_{SV} parameterizations used. When examining the distributions of the mean winter and summer POA concentrations in the SOAP and VBS_3POA experiments, a qualitative similarity can be observed with the corresponding distributions in CSwI and CVb. The quantitative differences between these distributions can be attributed to the use of different emission inventories since Jiang et al. (2021) employed the emission inventory TNO_MACC-III (Kuenen et al., 2014), the predecessor of CAMS-REG-v4.2 that does not account for SVOC emissions. The more apparent differences in the mean winter POA concentrations between CVb and VBS_3POA over Italy could be ascribed mainly to the above-mentioned overestimation of POA in CVb over this area. The distributions of the mean winter and summer SOA concentrations in the SOAP and VBS_3POA experiments exhibit distinct patterns compared to those in CSwI and CVb, particularly over some regions in Germany, Poland, and the Czech Republic. These differences, which can reach up to about 2–3 $\mu g\,m^{-3}$ during both seasons, could be mainly caused by the use of different amounts of biogenic emissions, especially monoterpene emissions. To substantiate this claim, it is noteworthy that Jiang et al. (2021) utilized the PSI model developed at the Laboratory of Atmospheric Chemistry of the Paul Scherrer Institute (Andreani-Aksoyoglu and Keller, 1995; Oderbolz et al., 2013; Jiang et al., 2019a) to estimate biogenic emissions. Furthermore, Jiang et al. (2019a) demonstrated that the biogenic emissions, particularly monoterpene emissions, estimated by the PSI model result in substantially higher SOA production than the biogenic emissions derived from the MEGAN model. Notably, the regions with the most pronounced differences in SOA production include, among others, the mentioned regions of Central Europe.

3.2.2 Comparison with measurements

Figure S5 in the Supplement compares the observed and modeled mean daily OC concentrations at the Prague–Suchdol and Košetice stations during the individual seasons. Figure S6 in the Supplement presents these comparisons at the stations utilized in both campaigns during their winter and summer phases. Figure 6 depicts the differences between the modeled and observed mean daily OC concentrations at the Prague–Suchdol and Košetice stations in the individual seasons. Figure 7 illustrates these differences at the stations utilized in both campaigns during their winter and summer phases. Table S9 in the Supplement offers the statistical comparison of the modeled and observed mean daily OC concentrations at the Prague–Suchdol and Košetice stations, while Table S10 in the Supplement provides the same statistical analysis for the stations utilized in both campaigns.

All these figures and the MB values in both tables indicate that the model in all the experiments generally more or less underestimates the daily OC concentrations at all the stations during all the periods of comparison. At the same time, several qualitative similarities can be seen in all these comparisons. First, CSnI and SSnI typically underestimate these concentrations similarly, with slightly more pronounced differences during the summer. Second, CSwI and SSwI tend to underestimate these concentrations similarly, again with slightly more pronounced differences in the summer. Additionally, they underestimate the concentrations slightly less than their corresponding experiments without additional IVOC emissions (i.e., CSnI and SSnI,

https://doi.org/10.5194/egusphere-2025-167
Preprint. Discussion started: 25 April 2025

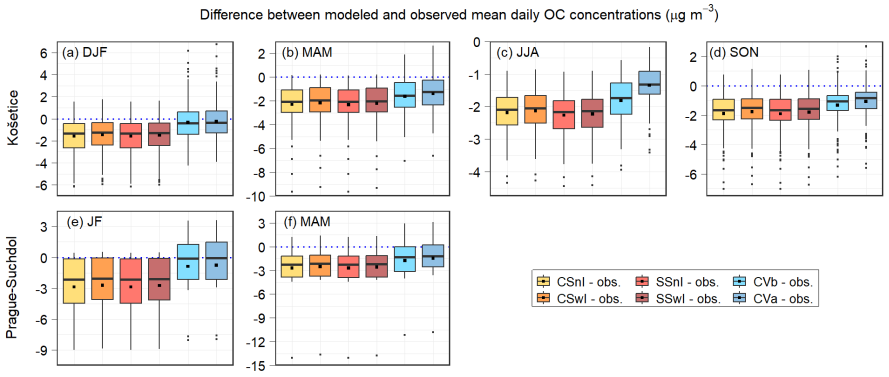

Figure 6. Differences between the modeled and observed mean daily OC concentrations at the Košetice station during the winter **(a)**, spring **(b)**, summer **(c)**, and autumn **(d)** seasons of 2018 and 2019 and at the Prague–Suchdol station during January and February 2018 **(e)** and the spring of 2018 **(f)**. The differences for all the model experiments of the first sensitivity analysis are depicted.

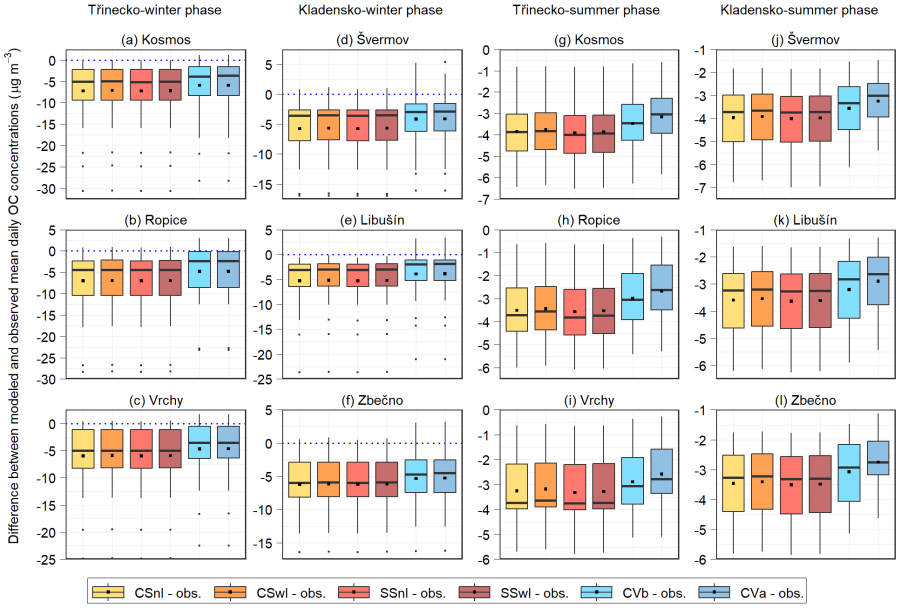

Figure 7. Differences between the modeled and observed mean daily OC concentrations at the Kosmos, Ropice, and Vrchy stations in the Třinecko area during the winter **(a–c)** and summer **(g–i)** phase of the campaign and at the Švermov, Libušín, and Zbečno stations in the Kladensko area during the winter **(d–f)** and summer **(j–l)** phase of the campaign. The differences for all the model experiments of the first sensitivity analysis are depicted.

respectively). Third, CVb underestimates these concentrations even less than CSwI and SSwI. Finally, CVa underestimates them even less than CVb, especially in the summer. This trend aligns with the seasonal distributions of POA and SOA described

https://doi.org/10.5194/egusphere-2025-167
Preprint. Discussion started: 25 April 2025

above. Moreover, Tables S4 and S6 show a similar pattern of improving the model predictions of the daily OC concentrations in these experiments in terms of all the other statistical measures used.

The values of all the statistical metrics used further demonstrate that the quality of the prediction of these concentrations is influenced by both the location within the domain and the period. The values of NMSE, IOA, and FAC2 at the stations used in both campaigns (Table S10) indicate a better prediction in all the experiments during the winter phases (NMSE = 84.2—447.2 %, IOA = 0.46—0.58, FAC2 = 12.9—68.6 %) than in the summer phases (NMSE = 114.2—653.8 %, IOA = 0.36—0.49, FAC2 = 0—31 %). At the same time, they show that the winter phases are slightly better predicted in the Kladensko area, while the summer phases are slightly better predicted in the Třinecko area. However, it is worth noting the FAC2 values determined even for the best-predicting experiment (CVa) are very low (0–31 %) during the summer phases at all these stations.

The values of all the statistical metrics indicate that the model predictions of the mean daily OC concentrations at the Prague–Suchdol (NMSE = 33.2–82.4 %, IOA = 0.63–0.78, FAC2 = 60–86.7 %) and Košetice (NMSE = 21.5–59 %, IOA = 0.63–0.85, FAC2 = 64.2–83.8 %) stations (Table S9) are considerably more accurate in all the experiments during the winter seasons than those at the stations in the Kladensko and Třinecko areas during their winter phases. These findings could be partly explained by the more pronounced differences between the modeled and measured wind speeds at the campaign stations. During the summer seasons, a similar conclusion to the one mentioned above applies for the Košetice station (NMSE = 48.1–240.4 %, IOA = 0.38–0.53, FAC2 = 0–61.8 %), especially in CVb and CVa. In order to make similar comparisons over the identical periods, we calculated all the metrics for the Košetice station corresponding to the periods of the individual phases of both campaigns, except for the summer phase in the Třinecko area due to missing data (Table S9). The comparisons of these metrics with those determined for the stations in both campaigns (Table S10) lead to the same conclusions that we stated above.

The comparison of NMSE, IOA, and FAC2 at the Prague–Suchdol station shows that the predictions of the mean daily OC concentrations in all the experiments are more accurate during the winter season than during the spring season (NMSE = 56.4–153.0 %, IOA = 0.38–0.50, FAC2 = 47.8–65.2 %). Similar comparisons at the Košetice station also show that these concentrations are best predicted in all the experiments during the winter seasons. In contrast, they are predominantly predicted least accurately at this station during the summer seasons.

Finally, taking into account the values of all the mentioned statistical measures at all the stations considered here, as well as all the distributions of differences between the modeled and observed mean daily OC concentrations, we can state that daily OC concentrations are most accurately modeled in CVa, followed by CVb. In other words, the best modeled daily OC concentrations, although still underestimated, were achieved by simultaneously supplying estimates of both IVOC and SVOC emissions to the simulation in which OA chemistry was handled by the 1.5-D VBS scheme with activated aging processes of POA and SOA from all anthropogenic sources as well as SOA from biogenic sources.

3.3 Sensitivity on chemical boundary conditions

To present and discuss the results of this sensitivity analysis, we adopt a similar approach to that utilized for the previous sensitivity study. Thus, we first investigate the spatial distributions of the mean seasonal impacts on the concentrations of POA and SOA in the experiments of this sensitivity analysis during both seasons, using the same definition of these impacts as in

https://doi.org/10.5194/egusphere-2025-167
Preprint. Discussion started: 25 April 2025

the first sensitivity study. Subsequently, we evaluate the OC concentrations obtained from the individual experiments of this sensitivity analysis.

3.3.1 Spatial distributions of POA and SOA

Figures 8a and b show the spatial distributions of the mean seasonal concentrations of POA in both reference experiments (CSwI and CVb) during the winters and summers, respectively. As we showed in the first sensitivity analysis, these distributions in CSwI are almost identical to those in CSnI during both seasons (Figs. 4a and b). At the same time, the distributions in CVb exhibit similar spatial patterns to those in CSwI during both seasons, but they differ in magnitude. Specifically, the highest mean seasonal POA concentrations in CSwI reach up to 9 $\mu g\,m^{-3}$ during the winters and up to 1.5 $\mu g\,m^{-3}$ during the summers, whereas in CVb, these concentrations peak at 19 $\mu g\,m^{-3}$ during the winters and 2.2 $\mu g\,m^{-3}$ during the summers.

Figures 8c and d illustrate the spatial distributions of the mean seasonal impacts on POA concentrations during the winters and summers, respectively. Moreover, Table S8 includes the values of the domain-averaged mean seasonal impacts on POA concentrations (ΔPOA). When OA is represented as SOA at the boundaries of the model domain, the mean seasonal impacts on POA concentrations in Sp0s100 are minor in both seasons. In Vp0s100, these impacts during both seasons typically reach values up to 0.25 $\mu g\,m^{-3}$, with somewhat more pronounced effects observed in the winters. This phenomenon may be attributed to the SOA supplied, which likely shifts the thermodynamic balance in the redistribution of POM_{SV} between the gas and aerosol phases toward the aerosol phase. The subsequent increase in the share of POA in OA at the boundaries of the model domain in Sp50s50 and Sp100s0 (and analogously in Vp50s50 and Vp100s0) is manifested by a gradual rise in the mean seasonal impacts across the entire model domain during both seasons. The spatial distributions of the mean winter impacts in these model experiments feature asymmetric gradients predominantly oriented from the Alps toward the western, southern, and eastern boundaries. These gradients are further influenced locally by other mountain ranges, such as the High Tatras. The spatial distribution of the mean summer impacts exhibits a similar structure, with pronounced gradients extending toward all domain boundaries. As can be seen from the shape of these distributions and the values of ΔPOA, the increase in the mean seasonal impacts during both seasons is consistently higher in the experiments in which SOAP handles OA chemistry. This phenomenon can be attributed to the fact that in Vp50s50 and Vp100s0, a portion of POA evaporates into the gas phase, a process that does not occur in Sp50s50 and Sp100s0. The mean seasonal impacts and their domain-averaged values in both Sp50s50 and Vp50s50 are higher during the summer seasons (ΔPOA = 1.71 and 1.29 $\mu g\,m^{-3}$, respectively) than in the winter seasons (ΔPOA = 0.69 and 0.63 $\mu g\,m^{-3}$, respectively). Similarly, the mean seasonal impacts and their domain-averaged values in both Sp100s0 and Vp100s0 are also higher during the summer seasons (ΔPOA = 3.45 and 3.10 $\mu g\,m^{-3}$, respectively) than in the winter seasons (ΔPOA = 1.37 and 1.17 $\mu g\,m^{-3}$, respectively).

The spatial distributions of the mean seasonal concentrations of SOA in both reference experiments during the winters and summers are depicted in Figs. 9a and b, respectively. Similar to the spatial distributions of the mean winter POA concentrations, the mean winter SOA concentrations exhibit a similar spatial pattern in both experiments; however, they differ in magnitudes. While these concentrations usually range between 0.1–1.25 $\mu g\,m^{-3}$ in CSwI, they vary between 0.2–3.75 $\mu g\,m^{-3}$ in CVb. In contrast, the spatial distributions of the mean summer SOA concentrations in both experiments differ not only in size but also

https://doi.org/10.5194/egusphere-2025-167
Preprint. Discussion started: 25 April 2025

in the geographical locations of the areas with the highest values. In CSwI, the mean summer SOA concentrations typically range between 0.4–1.75 $\mu g\,m^{-3}$, with the highest values being reached mainly in the southern area of the Pannonian Basin. In CVb, these concentrations usually vary between 0.8–3.5 $\mu g\,m^{-3}$, with the highest values found in the Po Valley and southern Germany.

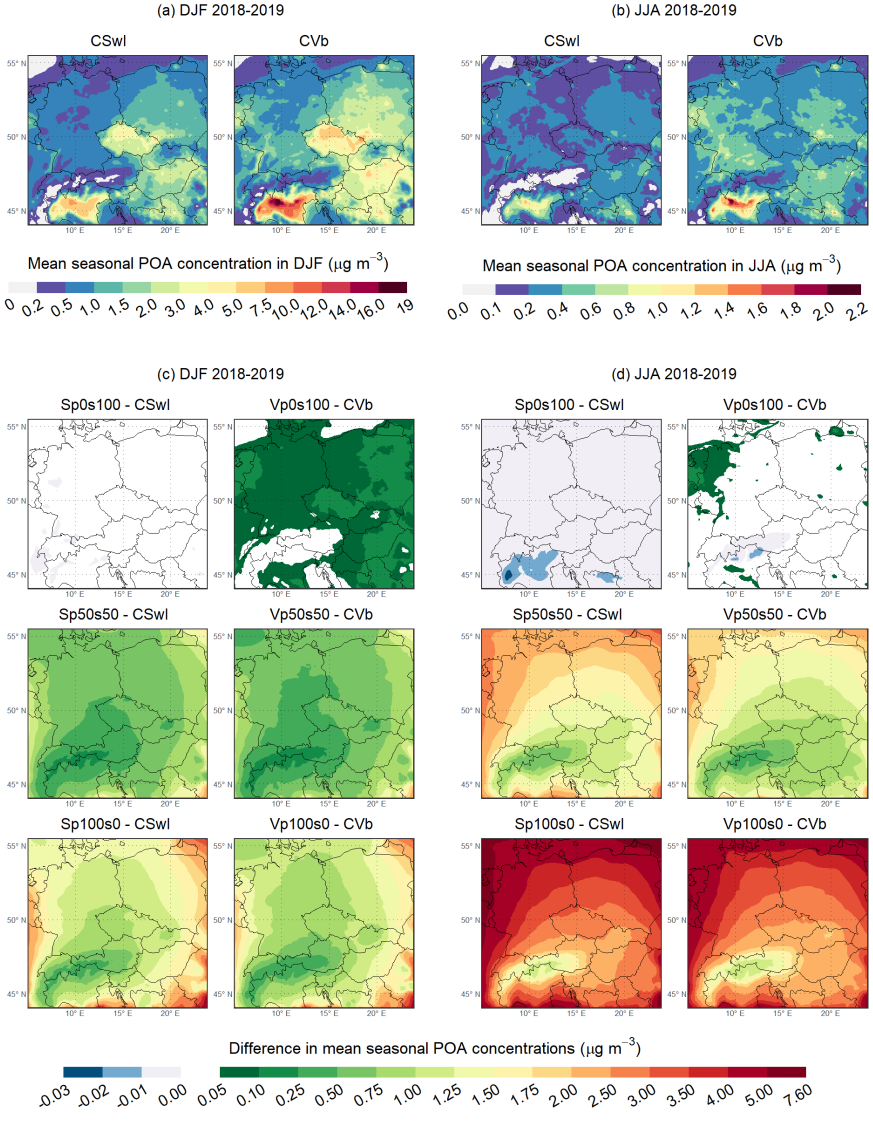

Figure 8. Mean seasonal POA concentration (in $\mu g\,m^{-3}$) in the reference experiments of the second sensitivity analysis (CSwI and Cvb) during the winter **(a)** and summer **(b)** seasons of 2018 and 2019. The difference between the mean seasonal POA concentration predicted in the individual experiments of the second sensitivity analysis and its counterpart in the corresponding reference (CSwI or Cvb) experiment (in $\mu g\,m^{-3}$) during the winter **(c)** and summer **(d)** seasons of 2018 and 2019.

https://doi.org/10.5194/egusphere-2025-167
Preprint. Discussion started: 25 April 2025

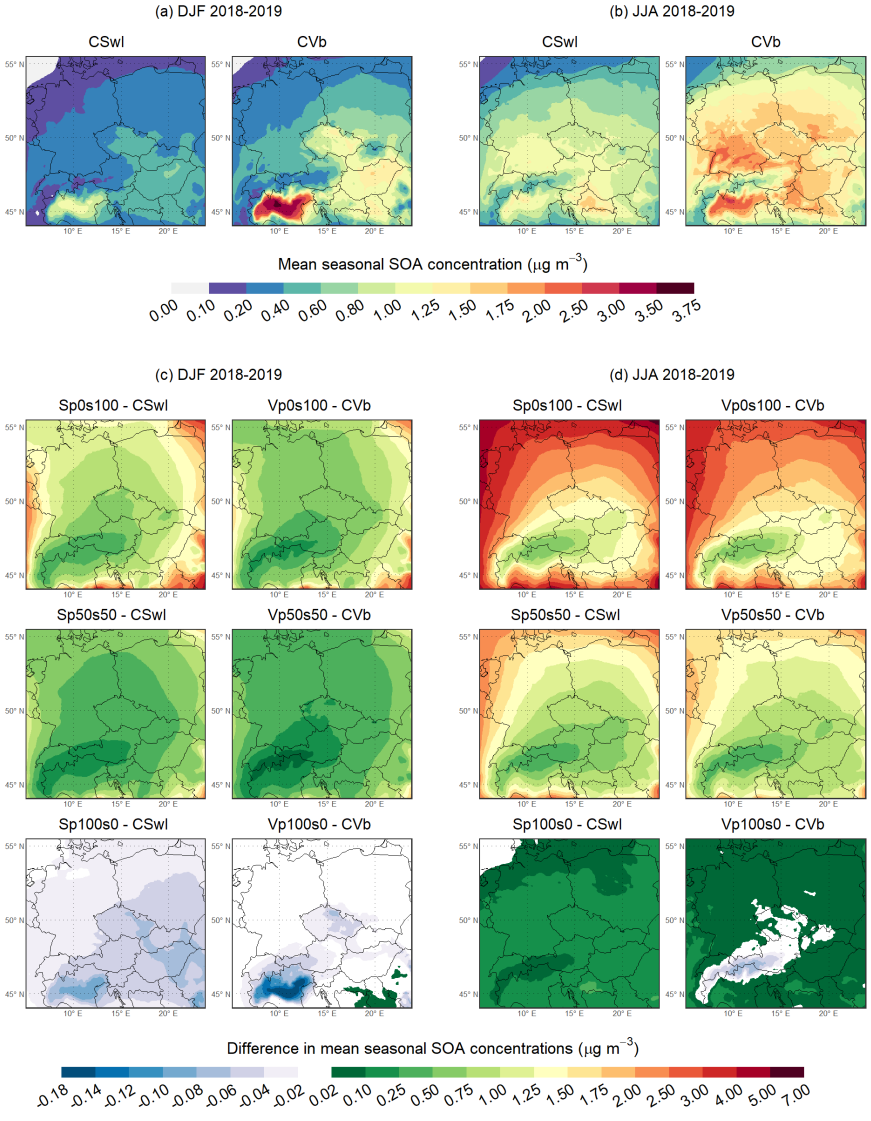

Figure 9. Same as Fig. 8 but for SOA.

Finally, as for the mean seasonal impacts on SOA concentrations, Figs. 9c and d show their spatial distributions during the winters and summers, respectively. Furthermore, the values of the domain-averaged mean seasonal impacts on SOA concentrations are provided in Table S8 in the Supplement. When OA is represented as POA at the boundaries of the model domain, the mean winter impacts in Sp100s0 are negative, decreasing to -0.1 $\mu g\,m^{-3}$. In Vp100s0, they are also negative above most of the domain, dropping to -0.18 $\mu g\,m^{-3}$. On the contrary, the mean summer impacts in Sp100s0 are positive, reaching up to 0.5 $\mu g\,m^{-3}$. In Vp100s0, except for the Alps and High Tatras, they are similarly positive, reaching up to 0.5 $\mu g\,m^{-3}$. The observed impacts in these simulations are likely linked to changes in other pollutant(s) at the boundaries of the model domain,

https://doi.org/10.5194/egusphere-2025-167
Preprint. Discussion started: 25 April 2025

which influence SOA chemistry. The spatial distributions of the mean seasonal impacts on SOA concentrations in Sp50s50 and Sp0s100 (and similarly in Vp50s50 and Vp0s100) exhibit structures akin to those observed for the mean seasonal impacts on POA concentrations in Sp50s50 and Sp100s0 (and likewise in Vp50s50 and Vp50s000) (Figs. 8c and d) during both seasons. The patterns of these distributions, along with the values of ΔSOA, indicate that the increase in the mean seasonal impacts as the proportion of SOA in OA at boundaries increases is consistently higher during both seasons in experiments where SOAP handles OA chemistry. This phenomenon is presumably also conditioned by the fact that a portion of POA evaporates in Vp50s50 and Vp0s100, which does not occur in Sp50s50 and Sp0s100. The mean seasonal impacts and their domain-averaged values in both Sp50s50 and Vp50s50 are higher in the summers (Δ SOA = 1.22 and 1.15 $\mu g\,m^{-3}$, respectively) than in the winters (Δ SOA = 0.55 and 0.41 $\mu g\,m^{-3}$, respectively). Similarly, the mean seasonal impacts and their domain-averaged values in both Sp0s100 and Vp0s100 are also higher in the summers (Δ SOA = 2.27 and 2.03 $\mu g\,m^{-3}$, respectively) than in the winters (Δ SOA = 1.15 and 0.83 $\mu g\,m^{-3}$, respectively).

3.3.2 Comparison with measurements

The observed and modeled mean daily OC concentrations at the Prague–Suchdol and Košetice stations in the individual seasons are compared in Fig. S7 in the Supplement. Figure S8 in the Supplement shows these comparisons at the stations employed in both campaigns during their winter and summer phases. Figure 10 depicts the differences between the modeled and observed mean daily OC concentrations at the Prague–Suchdol and Košetice stations in the individual seasons. Figure 11 illustrates these differences at the stations utilized in both campaigns during their winter and summer phases. The statistical comparison of the modeled and observed mean daily OC concentrations at the Prague–Suchdol and Košetice stations is provided in Table S11. Tables S12 and S13 in the Supplement supply the same statistical analysis for the stations utilized in both campaigns.

All these figures and the MB values in the tables show the detected underestimations of the mean daily OC concentrations in both reference experiments, which we discussed in Sect. 3.2.2. At the same time, they demonstrate that incorporating OA into the chemical boundary conditions reduces these underestimations at all the stations during all the periods, resulting in

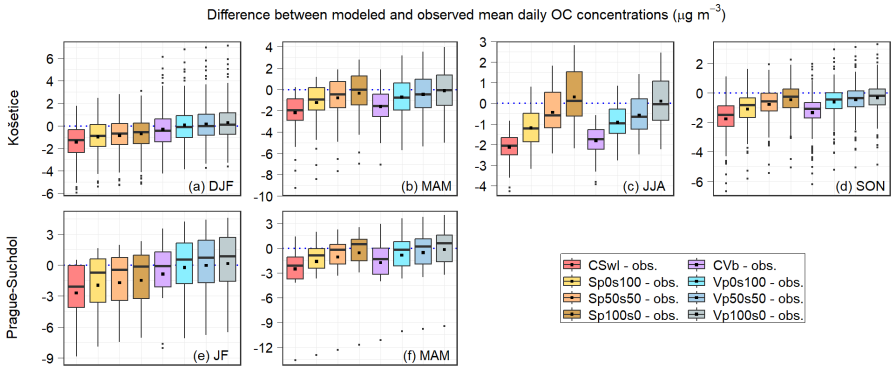

Figure 10. Same as Fig. 6 but for the experiments of the second sensitivity analysis.

https://doi.org/10.5194/egusphere-2025-167
Preprint. Discussion started: 25 April 2025

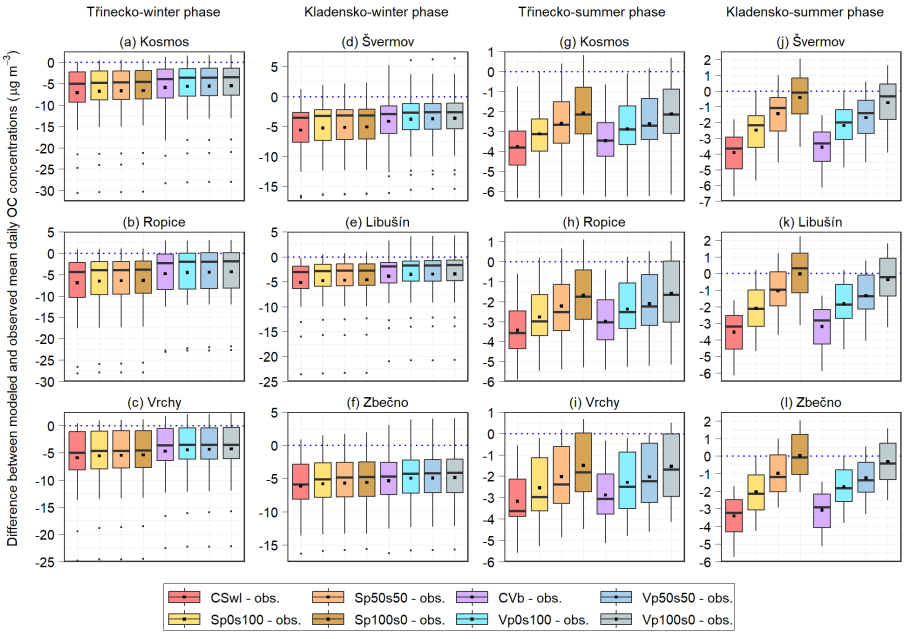

Figure 11. Same as Fig. 7 but for the experiments of the second sensitivity analysis.

enhanced model predictions of the analyzed concentrations. The magnitude of these reductions consistently increases with the increase in the share of POA in OA at the boundaries of the model domain. Moreover, in some cases, this incorporation even leads to slight overestimations of the mean daily OC concentrations, e.g., at the Košetice station in (1) Vp0s100, Vp50s50, and Vp100s0 during the winter seasons (Figs. 10a and S7a, Table S11) and (2) Sp100s0 and Vp100s0 during the summer seasons (Figs. 10c and S7c, Table S11).

Tables S11-13 further indicate that with the increase in the share of POA in OA at the boundaries of the model domain, there is always a gradual improvement of all the statistical metrics investigated at all the stations. This trend aligns with expectations, at least during the winter and summer seasons (phases), given the underestimations of the analyzed concentrations in the reference experiments and the trends in the spatial distributions of OA (Fig. S9 in the Supplement), the components of which we detailed in the previous subsection. The FAC2 values reveal that the most pronounced improvements in the modeled concentrations occur mainly during the summer seasons, especially at the stations in the Kladensko area and at the Košetice station. Concretely, the FAC2 at the stations in the Kladensko area improved from 0–3.3 % to 50–100 %, while at the Košetice station, the FAC2 increased from 0–16.7 % to 59.8–92.2 %.

4 Conclusions

This study provides, in the form of two sensitivity analyses, a comprehensive examination of the modeling of organic aerosols over Central Europe, focusing on the roles of IVOC and SVOC emissions and chemical boundary conditions. The first sensi-

https://doi.org/10.5194/egusphere-2025-167
Preprint. Discussion started: 25 April 2025

tivity analysis demonstrated that source-specific and non-source-specific estimates of IVOC and SVOC emissions substantially affect the modeled concentrations of both POA and SOA. A comparison of modeled daily OC concentrations with measurements at stations in the Czech Republic showed that the model best reproduces these concentrations in the case when the OA chemistry is controlled by the 1.5-D VBS scheme with activated aging processes of POA and SOA from all anthropogenic sources as well as SOA from biogenic sources. This finding is due to the fact that the model at this setting most significantly reduces the underestimation of OC, which is present in all experiments of this sensitivity analysis. Additionally, the comparison indicated that the model predicts the daily OC concentrations more accurately in winter than in summer, with the accuracy of the predictions varying by station location.

The second sensitivity analysis provided valuable insights into the contributions of OA sources from around Central Europe to the concentrations of OA, POA, and SOA in this region, or rather about the uncertainties of these contributions due to the lack of knowledge of the share of POA (or SOA) in OA at the edges of the model domain. A comparison of modeled daily OC concentrations with measurements at stations in the Czech Republic showed that incorporating OA into the chemical boundary conditions improves model predictions at all the stations. At the same time, the rate of this improvement increases with the growing share of POA in OA at the boundaries of the model domain. In terms of FAC2, the most pronounced improvements in the modeled OC concentrations occur mainly during the summer seasons, which points to the essential influence of OA from the boundaries of the model domain, especially during this season.

In the study, we have identified several shortcomings that we will address in future research. For instance, it is necessary to increase the temporal resolution of chemical boundary conditions and, ideally, to use those that directly contain POA and SOA concentrations. Further, it is important to substantially increase the horizontal resolution of the domain, which could help reduce wind speed overestimations. It is also essential to consider the uncertainties of many factors, such as source-specific parameterizations for IVOC and SVOC emission estimates, volatility distributions of SVOC emissions, rate constants of aging processes, or the emissions of BVOCs.

Appendix A: SOAP and 1.5-D VBS

Here, we briefly describe both modules that govern the OA chemistry in CAMx version 7.10. More information can be found in Ramboll (2020).

SOAP version 2.2 treats POA using the traditional assumptions mentioned in the introduction; thus, it considers POA to be a single non-volatile species that does not evolve chemically. Further, it considers the oxidation of four anthropogenic gaseous species (benzene, toluene, xylene, and anthropogenic IVOC) to form two condensable gas (CG) species (more-volatile and less-volatile) and one non-volatile species in the aerosol phase. Similarly, the oxidation of three biogenic volatile organic compounds (BVOCs) (isoprene, monoterpenes, and sesquiterpenes) is considered to form two CG species (more-volatile and less-volatile) and one non-volatile species; however, these species are different from those created from the anthropogenic precursors. At the same time, the more-volatile and less-volatile CG species resulting from both anthropogenic and biogenic

https://doi.org/10.5194/egusphere-2025-167
Preprint. Discussion started: 25 April 2025

precursors are redistributed between the gas and aerosol phases following the pseudo-ideal solution theory (Strader et al., 1999).

The 1.5-D VBS scheme uses five basis sets to represent different degrees of oxidation in ambient OA: three basis sets for freshly emitted OA (originating from meat cooking, other anthropogenic sources, and biomass burning) and two basis sets for chemically aged, oxygenated OA (including both anthropogenic and biogenic sources). Each basis set comprises five volatility bins, ranging from 10^{-1} to 10^{3} $\mu g\,m^{-3}$ in saturation concentration, which approximately encompasses the volatility range of SVOCs. The chemical aging of OA is modeled by redistributing OA mass along predefined pathways within and between these basis sets, decreasing its volatility while simultaneously increasing its oxidation state. The gas-phase hydroxyl radical reaction rates for the chemical aging of POA and anthropogenic SOA, except those originating from biomass burning, are assumed to be 4×10^{-11} and 2×10^{-11} $cm^3\,molecule^{-1}\,s^{-1}$, respectively. In contrast, the chemical aging of biogenic SOA and SOA originating from biomass burning (both anthropogenic and biogenic) is disabled. The 1.5-D VBS scheme incorporates the oxidation of traditional anthropogenic and biogenic gaseous precursors of SOA utilized in SOAP, including benzene, toluene, xylene, isoprene, monoterpenes, and sesquiterpenes. Similarly to SOAP, this module also considers the oxidation of IVOCs. However, unlike SOAP, in which one surrogate species represents all anthropogenic IVOC emissions, this module uses four surrogate species for source-specific IVOC emissions (specifically, for IVOC emissions from gasoline vehicles, diesel vehicles, other anthropogenic sources, and biomass burning). Also, unlike SOAP, which maps POA emissions from all anthropogenic sources to a single aerosol species, the 1.5-D VBS scheme assigns POA emissions to the individual surrogate OA species within the volatility basis sets. This allocation is based on five source-specific volatility distribution factors, which correspond to POA emissions from gasoline vehicles, diesel vehicles, meat cooking, other anthropogenic sources, and biomass burning. At the same time, it means that the 1.5-D VBS scheme implicitly assumes that POA emissions from relevant sources should contain POM_{SV}.

Code and data availability. CAMx version 7.10 is available at http://camx-wp.azurewebsites.net/download/source (Ramboll, 2021). WRF version 4.2 can be downloaded from https://github.com/wrf-model/WRF/releases (WRF, 2020). MEGAN version 2.10 can be obtained from https://bai.ess.uci.edu/megan/data-and-code/megan21 (Guenther et al., 2014). The FUME emission model can be found at https://doi.org/10.5281/zenodo.10142912 (Belda et al., 2023). OC measurements at the Koetice station can be obtained from the EBAS database available at https://ebas-data.nilu.no/default.aspx (EBAS, 2025). All meteorological data used in the paper can be obtained from the Czech Hydrometeorological Institute (CHMI; https://www.chmi.cz). The CAMS global reanalysis (EAC4) monthly averaged fields can be downloaded from https://ads.atmosphere.copernicus.eu/datasets/cams-global-reanalysis-eac4-monthly?tab=download (ADS, 2025). The Czech REZZO and ATEM emission data can be obtained on request from their publishers, the CHMI and the Studio of Ecological Models (https://www.atem.cz), respectively. The complete model configuration and all the simulated data (1-dimensional hourly data) used for the analysis are stored at the Department of Atmospheric Physics of the Charles University data storage facilities (about 3TB) and are available upon request from the main author.

https://doi.org/10.5194/egusphere-2025-167
Preprint. Discussion started: 25 April 2025

Author contributions. LB performed the simulations, analyzed and validated the modeled data, and wrote most of the text. PH and JK contributed to setting up the model simulations and writing the text. JP and OV helped with the methodology, and PV carried out and processed the OC measurements at the Prague–Suchdol station.

Competing interests. The authors declare that they have no conflict of interest.

Acknowledgements. This work has been funded by the Czech Technological Agency (TACR) grant No.SS02030031 ARAMIS (Air Quality Research Assessment and Monitoring Integrated System) and partly by the project of the Charles University SVV no. 260709 and by the Project OP JAK "Natural and anthropogenic georisks" CZ.02.01.014/0022_008/0004605. We also acknowledge the CAMS-REG-v4.2 emission data and the CAMS global reanalysis (EAC4) monthly averaged fields provided by the Copernicus Atmosphere Monitoring Service; the REZZO dataset, the OC measurements from the campaigns in the Třinecko and Kladensko areas, and all the meteorological data provided by the Czech Hydrometeorological Institute; the OC measurements at the Prague–Suchdol station provided by the Institute of Chemical Process Fundamentals of the Czech Academy of Science; the ATEM Traffic Emissions dataset provided by ATEM (Studio of Ecological Models), and the ERA-Interim reanalysis provided by the European Centre for Medium-Range Weather Forecast. We also acknowledge the providers of the EBAS database, the Norwegian Institute for Air Research (NILU), and the Co-operative Programme for Monitoring and Evaluation of the Long-range Transmission of Air Pollutants in Europe (EMEP) for providing OC measurements at the Košetice station.

https://doi.org/10.5194/egusphere-2025-167
Preprint. Discussion started: 25 April 2025

References

ADS: CAMS global reanalysis (EAC4) monthly averaged fields [data set], https://ads.atmosphere.copernicus.eu/datasets/cams-global-reanalysis-eac4-monthly?tab=download, last access: 11 January 2025, 2025.

Ain, N. U. and Qamar, S. U. R.: Particulate Matter-Induced Cardiovascular Dysfunction: A Mechanistic Insight, Cardiovascular Toxicology, 21, 505–516, https://doi.org/10.1007/s12012-021-09652-3, 2021.

Aksoyoglu, S., Keller, J., Barmpadimos, I., Oderbolz, D., Lanz, V. A., Prévôt, A. S. H., and Baltensperger, U.: Aerosol modelling in Europe with a focus on Switzerland during summer and winter episodes, Atmospheric Chemistry and Physics, 11, 7355–7373, https://doi.org/10.5194/acp-11-7355-2011, 2011.

Andreani-Aksoyoglu, S. and Keller, J.: Estimates of monoterpene and isoprene emissions from the forests in Switzerland, Journal of Atmospheric Chemistry, 20, 71–87, https://doi.org/10.1007/BF01099919, 1995.

Arias-Pérez, R. D., Taborda, N. A., Gómez, D. M., Narvaez, J. F., Porras, J., and Hernandez, J. C.: Inflammatory effects of particulate matter air pollution, Environmental Science and Pollution Research, 27, 42 390–42 404, https://doi.org/10.1007/s11356-020-10574-w, 2020.

Arola, A., Lipponen, A., Kolmonen, P., Virtanen, T. H., Bellouin, N., Grosvenor, D. P., Gryspeerdt, E., Quaas, J., and Kokkola, H.: Aerosol effects on clouds are concealed by natural cloud heterogeneity and satellite retrieval errors, Nature Communications, 13, https://doi.org/10.1038/s41467-022-34948-5, 2022.

Bartík, L., Huszár, P., Karlický, J., Vlček, O., and Eben, K.: Modeling the drivers of fine PM pollution over Central Europe: impacts and contributions of emissions from different sources, Atmospheric Chemistry and Physics, 24, 4347–4387, https://doi.org/10.5194/acp-24-4347-2024, 2024.

Belda, M., Krč, P., Resler, J., Huszár, P., Benešová, N., Karlický, J., and Juruš, P.: FUME-dev/fume: Official 2.0 release (2.0), Zenodo [code], https://doi.org/10.5281/zenodo.10142912, last access: 11 January 2025, 2023.

Belda, M., Benešová, N., Resler, J., Huszár, P., Vlček, O., Krč, P., Karlický, J., Juruš, P., and Eben, K.: FUME 2.0 – Flexible Universal processor for Modeling Emissions, Geoscientific Model Development, 17, 3867–3878, https://doi.org/10.5194/gmd-17-3867-2024, 2024.

Benešová, N., Belda, M., Eben, K., Geletič, J., Huszár, P., Juruš, P., Krč, P., Resler, J., and Vlček, O.: New open source emission processor for air quality models, in: Proceedings of Abstracts 11th International Conference on Air Quality Science and Application, edited by Sokhi, R., Tiwari, P. R., Gállego, M. J., Craviotto Arnau, J. M., Castells Guiu, C., and Singh, V., p. 22, Published by University of Hertfordshire, https://doi.org/10.18745/PB.19829, paper presented at Air Quality 2018 conference, Barcelona, 12-16 March, 2018.

Bressi, M., Sciare, J., Ghersi, V., Bonnaire, N., Nicolas, J. B., Petit, J.-E., Moukhtar, S., Rosso, A., Mihalopoulos, N., and Féron, A.: A one-year comprehensive chemical characterisation of fine aerosol ($PM_{2.5}$) at urban, suburban and rural background sites in the region of Paris (France), Atmospheric Chemistry and Physics, 13, 7825–7844, https://doi.org/10.5194/acp-13-7825-2013, 2013.

Byun, D. and Schere, K. L.: Review of the Governing Equations, Computational Algorithms, and Other Components of the Models-3 Community Multiscale Air Quality (CMAQ) Modeling System, Applied Mechanics Reviews, 59, 51–77, https://doi.org/10.1115/1.2128636, 2006.

Carter, W. P.: Development of the SAPRC-07 chemical mechanism, Atmospheric Environment, 44, 5324–5335, https://doi.org/10.1016/j.atmosenv.2010.01.026, 2010.

Cavalli, F., Viana, M., Yttri, K. E., Genberg, J., and Putaud, J.-P.: Toward a standardised thermal-optical protocol for measuring atmospheric organic and elemental carbon: the EUSAAR protocol, Atmospheric Measurement Techniques, 3, 79–89, https://doi.org/10.5194/amt-3-79-2010, 2010.

https://doi.org/10.5194/egusphere-2025-167
Preprint. Discussion started: 25 April 2025

Chang, J. S., Brost, R. A., Isaksen, I. S. A., Madronich, S., Middleton, P., Stockwell, W. R., and Walcek, C. J.: A three-dimensional Eulerian acid deposition model: Physical concepts and formulation, Journal of Geophysical Research: Atmospheres, 92, 14 681–14 700, https://doi.org/10.1029/JD092iD12p14681, 1987.

Chen, G., Canonaco, F., Tobler, A., Aas, W., Alastuey, A., Allan, J., Atabakhsh, S., Aurela, M., Baltensperger, U., Bougiatioti, A., De Brito, J. F., Ceburnis, D., Chazeau, B., Chebaicheb, H., Daellenbach, K. R., Ehn, M., El Haddad, I., Eleftheriadis, K., Favez, O., Flentje, H., Font, A., Fossum, K., Freney, E., Gini, M., Green, D. C., Heikkinen, L., Herrmann, H., Kalogridis, A.-C., Keernik, H., Lhotka, R., Lin, C., Lunder, C., Maasikmets, M., Manousakas, M. I., Marchand, N., Marin, C., Marmureanu, L., Mihalopoulos, N., Močnik, G., Nęcki, J., O'Dowd, C., Ovadnevaite, J., Peter, T., Petit, J.-E., Pikridas, M., Matthew Platt, S., Pokorná, P., Poulain, L., Priestman, M., Riffault, V., Rinaldi, M., Różański, K., Schwarz, J., Sciare, J., Simon, L., Skiba, A., Slowik, J. G., Sosedova, Y., Stavroulas, I., Styszko, K., Teinemaa, E., Timonen, H., Tremper, A., Vasilescu, J., Via, M., Vodička, P., Wiedensohler, A., Zografou, O., Cruz Minguillón, M., and Prévôt, A. S.: European aerosol phenomenology - 8: Harmonised source apportionment of organic aerosol using 22 Year-long ACSM/AMS datasets, Environment International, 166, 107 325, https://doi.org/10.1016/j.envint.2022.107325, 2022.

Ciarelli, G., Aksoyoglu, S., Crippa, M., Jimenez, J.-L., Nemitz, E., Sellegri, K., Äijälä, M., Carbone, S., Mohr, C., O'Dowd, C., Poulain, L., Baltensperger, U., and Prévôt, A. S. H.: Evaluation of European air quality modelled by CAMx including the volatility basis set scheme, Atmospheric Chemistry and Physics, 16, 10 313–10 332, https://doi.org/10.5194/acp-16-10313-2016, 2016.

Ciarelli, G., Aksoyoglu, S., El Haddad, I., Bruns, E. A., Crippa, M., Poulain, L., Äijälä, M., Carbone, S., Freney, E., O'Dowd, C., Baltensperger, U., and Prévôt, A. S. H.: Modelling winter organic aerosol at the European scale with CAMx: evaluation and source apportionment with a VBS parameterization based on novel wood burning smog chamber experiments, Atmospheric Chemistry and Physics, 17, 7653–7669, https://doi.org/10.5194/acp-17-7653-2017, 2017.

Crippa, M., Canonaco, F., Lanz, V. A., Äijälä, M., Allan, J. D., Carbone, S., Capes, G., Ceburnis, D., Dall'Osto, M., Day, D. A., DeCarlo, P. F., Ehn, M., Eriksson, A., Freney, E., Hildebrandt Ruiz, L., Hillamo, R., Jimenez, J. L., Junninen, H., Kiendler-Scharr, A., Kortelainen, A.-M., Kulmala, M., Laaksonen, A., Mensah, A. A., Mohr, C., Nemitz, E., O'Dowd, C., Ovadnevaite, J., Pandis, S. N., Petäjä, T., Poulain, L., Saarikoski, S., Sellegri, K., Swietlicki, E., Tiitta, P., Worsnop, D. R., Baltensperger, U., and Prévôt, A. S. H.: Organic aerosol components derived from 25 AMS data sets across Europe using a consistent ME-2 based source apportionment approach, Atmospheric Chemistry and Physics, 14, 6159–6176, https://doi.org/10.5194/acp-14-6159-2014, 2014.

Denier van der Gon, H. A. C., Bergström, R., Fountoukis, C., Johansson, C., Pandis, S. N., Simpson, D., and Visschedijk, A. J. H.: Particulate emissions from residential wood combustion in Europe – revised estimates and an evaluation, Atmospheric Chemistry and Physics, 15, 6503–6519, https://doi.org/10.5194/acp-15-6503-2015, 2015.

Donahue, N. M., Robinson, A. L., Stanier, C. O., and Pandis, S. N.: Coupled Partitioning, Dilution, and Chemical Aging of Semivolatile Organics, Environmental Science & Technology, 40, 2635–2643, https://doi.org/10.1021/es052297c, 2006.

Donahue, N. M., Robinson, A. L., and Pandis, S. N.: Atmospheric organic particulate matter: From smoke to secondary organic aerosol, Atmospheric Environment, 43, 94–106, https://doi.org/10.1016/j.atmosenv.2008.09.055, 2009.

Donahue, N. M., Epstein, S. A., Pandis, S. N., and Robinson, A. L.: A two-dimensional volatility basis set: 1. organic-aerosol mixing thermodynamics, Atmospheric Chemistry and Physics, 11, 3303–3318, https://doi.org/10.5194/acp-11-3303-2011, 2011.

Donahue, N. M., Kroll, J. H., Pandis, S. N., and Robinson, A. L.: A two-dimensional volatility basis set – Part 2: Diagnostics of organic-aerosol evolution, Atmospheric Chemistry and Physics, 12, 615–634, https://doi.org/10.5194/acp-12-615-2012, 2012.

EBAS: EBAS database, Norwegian Institute for Air Research (NILU) [data set], https://ebas-data.nilu.no/default.aspx, last access: 11 January 2025, 2025.

https://doi.org/10.5194/egusphere-2025-167
Preprint. Discussion started: 25 April 2025

Giani, P., Balzarini, A., Pirovano, G., Gilardoni, S., Paglione, M., Colombi, C., Gianelle, V. L., Belis, C. A., Poluzzi, V., and Lonati, G.: Influence of semi- and intermediate-volatile organic compounds (S/IVOC) parameterizations, volatility distributions and aging schemes on organic aerosol modelling in winter conditions, Atmospheric Environment, 213, 11–24, https://doi.org/10.1016/j.atmosenv.2019.05.061, 2019.

Guenther, A., Jiang, X., and Duhl, T.: MEGAN version 2.10, National Center for Atmospheric Research, Boulder, CO, USA [code], https://bai.ess.uci.edu/megan/data-and-code/megan21, last access: 11 January 2025, 2014.

Guenther, A. B., Jiang, X., Heald, C. L., Sakulyanontvittaya, T., Duhl, T., Emmons, L. K., and Wang, X.: The Model of Emissions of Gases and Aerosols from Nature version 2.1 (MEGAN2.1): an extended and updated framework for modeling biogenic emissions, Geoscientific Model Development, 5, 1471–1492, https://doi.org/10.5194/gmd-5-1471-2012, 2012.

Hertel, O., Berkowicz, R., Christensen, J., and Hov, Ø.: Test of two numerical schemes for use in atmospheric transport-chemistry models, Atmospheric Environment. Part A. General Topics, 27, 2591–2611, https://doi.org/10.1016/0960-1686(93)90032-T, 1993.

Hodzic, A., Jimenez, J. L., Madronich, S., Canagaratna, M. R., DeCarlo, P. F., Kleinman, L., and Fast, J.: Modeling organic aerosols in a megacity: potential contribution of semi-volatile and intermediate volatility primary organic compounds to secondary organic aerosol formation, Atmospheric Chemistry and Physics, 10, 5491–5514, https://doi.org/10.5194/acp-10-5491-2010, 2010.

Huszar, P., Karlický, J., Ďoubalová, J., Nováková, T., Šindelářová, K., Švábik, F., Belda, M., Halenka, T., and Žák, M.: The impact of urban land-surface on extreme air pollution over central Europe, Atmospheric Chemistry and Physics, 20, 11 655–11 681, https://doi.org/10.5194/acp-20-11655-2020, 2020.

Hutzell, W., Luecken, D., Appel, K., and Carter, W.: Interpreting predictions from the SAPRC07 mechanism based on regional and continental simulations, Atmospheric Environment, 46, 417–429, https://doi.org/10.1016/j.atmosenv.2011.09.030, 2012.

Inness, A., Ades, M., Agustí-Panareda, A., Barré, J., Benedictow, A., Blechschmidt, A.-M., Dominguez, J. J., Engelen, R., Eskes, H., Flemming, J., Huijnen, V., Jones, L., Kipling, Z., Massart, S., Parrington, M., Peuch, V.-H., Razinger, M., Remy, S., Schulz, M., and Suttie, M.: The CAMS reanalysis of atmospheric composition, Atmospheric Chemistry and Physics, 19, 3515–3556, https://doi.org/10.5194/acp-19-3515-2019, 2019.

Jathar, S. H., Gordon, T. D., Hennigan, C. J., Pye, H. O., Pouliot, G., Adams, P. J., Donahue, N. M., and Robinson, A. L.: Unspeciated organic emissions from combustion sources and their influence on the secondary organic aerosol budget in the United States, Proceedings of the National Academy of Sciences of the United States of America, 111(29), 10 473–8, https://doi.org/10.1073/pnas.1323740111, 2014.

Jiang, J., Aksoyoglu, S., Ciarelli, G., Oikonomakis, E., El-Haddad, I., Canonaco, F., O'Dowd, C., Ovadnevaite, J., Minguillón, M. C., Baltensperger, U., and Prévôt, A. S. H.: Effects of two different biogenic emission models on modelled ozone and aerosol concentrations in Europe, Atmospheric Chemistry and Physics, 19, 3747–3768, https://doi.org/10.5194/acp-19-3747-2019, 2019a.

Jiang, J., Aksoyoglu, S., El-Haddad, I., Ciarelli, G., Denier van der Gon, H. A. C., Canonaco, F., Gilardoni, S., Paglione, M., Minguillón, M. C., Favez, O., Zhang, Y., Marchand, N., Hao, L., Virtanen, A., Florou, K., O'Dowd, C., Ovadnevaite, J., Baltensperger, U., and Prévôt, A. S. H.: Sources of organic aerosols in Europe: a modeling study using CAMx with modified volatility basis set scheme, Atmospheric Chemistry and Physics, 19, 15 247–15 270, https://doi.org/10.5194/acp-19-15247-2019, 2019b.

Jiang, J., El Haddad, I., Aksoyoglu, S., Stefenelli, G., Bertrand, A., Marchand, N., Canonaco, F., Petit, J.-E., Favez, O., Gilardoni, S., Baltensperger, U., and Prévôt, A. S. H.: Influence of biomass burning vapor wall loss correction on modeling organic aerosols in Europe by CAMx v6.50, Geoscientific Model Development, 14, 1681–1697, https://doi.org/10.5194/gmd-14-1681-2021, 2021.

Jimenez, J. L., Canagaratna, M. R., Donahue, N. M., Prevot, A. S. H., Zhang, Q., Kroll, J. H., DeCarlo, P. F., Allan, J. D., Coe, H., Ng, N. L., Aiken, A. C., Docherty, K. S., Ulbrich, I. M., Grieshop, A. P., Robinson, A. L., Duplissy, J., Smith, J. D., Wilson, K. R., Lanz,

https://doi.org/10.5194/egusphere-2025-167
Preprint. Discussion started: 25 April 2025

V. A., Hueglin, C., Sun, Y. L., Tian, J., Laaksonen, A., Raatikainen, T., Rautiainen, J., Vaattovaara, P., Ehn, M., Kulmala, M., Tomlinson, J. M., Collins, D. R., Cubison, M. J., E., Dunlea, J., Huffman, J. A., Onasch, T. B., Alfarra, M. R., Williams, P. I., Bower, K., Kondo, Y., Schneider, J., Drewnick, F., Borrmann, S., Weimer, S., Demerjian, K., Salcedo, D., Cottrell, L., Griffin, R., Takami, A., Miyoshi, T., Hatakeyama, S., Shimono, A., Sun, J. Y., Zhang, Y. M., Dzepina, K., Kimmel, J. R., Sueper, D., Jayne, J. T., Herndon, S. C., Trimborn, A. M., Williams, L. R., Wood, E. C., Middlebrook, A. M., Kolb, C. E., Baltensperger, U., and Worsnop, D. R.: Evolution of Organic Aerosols in the Atmosphere, Science, 326, 1525–1529, https://doi.org/10.1126/science.1180353, 2009.

Karlický, J., Huszár, P., Nováková, T., Belda, M., Švábik, F., Ďoubalová, J., and Halenka, T.: The "urban meteorology island": a multi-model ensemble analysis, Atmospheric Chemistry and Physics, 20, 15 061–15 077, https://doi.org/10.5194/acp-20-15061-2020, 2020.

Koo, B., Knipping, E., and Yarwood, G.: 1.5-Dimensional volatility basis set approach for modeling organic aerosol in CAMx and CMAQ, Atmospheric Environment, 95, 158–164, https://doi.org/10.1016/j.atmosenv.2014.06.031, 2014.

Kuenen, J., Dellaert, S., Visschedijk, A., Jalkanen, J.-P., Super, I., and Denier van der Gon, H.: Copernicus Atmosphere Monitoring Service regional emissions version 4.2 (CAMS-REG-v4.2), Copernicus Atmosphere Monitoring Service, ECCAD, https://doi.org/10.24380/0vzb-a387, 2021.

Kuenen, J., Dellaert, S., Visschedijk, A., Jalkanen, J.-P., Super, I., and Denier van der Gon, H.: CAMS-REG-v4: a state-of-the-art high-resolution European emission inventory for air quality modelling, Earth System Science Data, 14, 491–515, https://doi.org/10.5194/essd-14-491-2022, 2022.

Kuenen, J. J. P., Visschedijk, A. J. H., Jozwicka, M., and Denier van der Gon, H. A. C.: TNO-MACC_II emission inventory; a multi-year (2003–2009) consistent high-resolution European emission inventory for air quality modelling, Atmospheric Chemistry and Physics, 14, 10 963–10 976, https://doi.org/10.5194/acp-14-10963-2014, 2014.

Lanz, V. A., Prévôt, A. S. H., Alfarra, M. R., Weimer, S., Mohr, C., DeCarlo, P. F., Gianini, M. F. D., Hueglin, C., Schneider, J., Favez, O., D'Anna, B., George, C., and Baltensperger, U.: Characterization of aerosol chemical composition with aerosol mass spectrometry in Central Europe: an overview, Atmospheric Chemistry and Physics, 10, 10 453–10 471, https://doi.org/10.5194/acp-10-10453-2010, 2010.

Li, J., Han, Z., Li, J., Liu, R., Wu, Y., Liang, L., and Zhang, R.: The formation and evolution of secondary organic aerosol during haze events in Beijing in wintertime, Science of The Total Environment, 703, 134 937, https://doi.org/10.1016/j.scitotenv.2019.134937, 2020.

Li, J., Carlson, B. E., Yung, Y. L., Lv, D., Hansen, J., Penner, J. E., Liao, H., Ramaswamy, V., Kahn, R. A., Zhang, P., Dubovik, O., Ding, A., Lacis, A. A., Zhang, L., and Dong, Y.: Scattering and absorbing aerosols in the climate system, Nature Reviews Earth & Environment, 3, 363–379, https://doi.org/10.1038/s43017-022-00296-7, 2022.

Liaskoni, M., Huszar, P., Bartík, L., Prieto Perez, A. P., Karlický, J., and Vlček, O.: Modelling the European wind-blown dust emissions and their impact on particulate matter (PM) concentrations, Atmospheric Chemistry and Physics, 23, 3629–3654, https://doi.org/10.5194/acp-23-3629-2023, 2023.

Lim, Y. B., Tan, Y., and Turpin, B. J.: Chemical insights, explicit chemistry, and yields of secondary organic aerosol from OH radical oxidation of methylglyoxal and glyoxal in the aqueous phase, Atmospheric Chemistry and Physics, 13, 8651–8667, https://doi.org/10.5194/acp-13-8651-2013, 2013.

Matsui, H., Koike, M., Kondo, Y., Takami, A., Fast, J. D., Kanaya, Y., and Takigawa, M.: Volatility basis-set approach simulation of organic aerosol formation in East Asia: implications for anthropogenic–biogenic interaction and controllable amounts, Atmospheric Chemistry and Physics, 14, 9513–9535, https://doi.org/10.5194/acp-14-9513-2014, 2014.

https://doi.org/10.5194/egusphere-2025-167
Preprint. Discussion started: 25 April 2025

Meroni, A., Pirovano, G., Gilardoni, S., Lonati, G., Colombi, C., Gianelle, V., Paglione, M., Poluzzi, V., Riva, G., and Toppetti, A.: Investigating the role of chemical and physical processes on organic aerosol modelling with CAMx in the Po Valley during a winter episode, Atmospheric Environment, 171, 126–142, https://doi.org/10.1016/j.atmosenv.2017.10.004, 2017.

Morgan, W. T., Allan, J. D., Bower, K. N., Highwood, E. J., Liu, D., McMeeking, G. R., Northway, M. J., Williams, P. I., Krejci, R., and Coe, H.: Airborne measurements of the spatial distribution of aerosol chemical composition across Europe and evolution of the organic fraction, Atmospheric Chemistry and Physics, 10, 4065–4083, https://doi.org/10.5194/acp-10-4065-2010, 2010.

Nenes, A., Pandis, S. N., and Pilinis, C.: ISORROPIA: A New Thermodynamic Equilibrium Model for Multiphase Multicomponent Inorganic Aerosols, Aquatic Geochemistry, 4, 123–152, https://doi.org/10.1023/A:1009604003981, 1998.

Nenes, A., Pandis, S. N., and Pilinis, C.: Continued development and testing of a new thermodynamic aerosol module for urban and regional air quality models, Atmospheric Environment, 33, 1553–1560, https://doi.org/10.1016/S1352-2310(98)00352-5, 1999.

Oderbolz, D. C., Aksoyoglu, S., Keller, J., Barmpadimos, I., Steinbrecher, R., Skjøth, C. A., Plaß-Dülmer, C., and Prévôt, A. S. H.: A comprehensive emission inventory of biogenic volatile organic compounds in Europe: improved seasonality and land-cover, Atmospheric Chemistry and Physics, 13, 1689–1712, https://doi.org/10.5194/acp-13-1689-2013, 2013.

Odum, J. R., Hoffmann, T., Bowman, F., Collins, D., Flagan, R. C., and Seinfeld, J. H.: Gas/particle partitioning and secondary organic aerosol yields, Environmental Science and Technology, 30, 2580–2585, https://doi.org/10.1021/es950943+, 1996.

Ortiz-Montalvo, D. L., Lim, Y. B., Perri, M. J., Seitzinger, S. P., and Turpin, B. J.: Volatility and Yield of Glycolaldehyde SOA Formed through Aqueous Photochemistry and Droplet Evaporation, Aerosol Science and Technology, 46, 1002–1014, https://doi.org/10.1080/02786826.2012.686676, 2012.

Pankow, J. F.: An absorption model of gas/particle partitioning of organic compounds in the atmosphere, Atmospheric Environment, 28, 185–188, https://doi.org/10.1016/1352-2310(94)90093-0, 1994.

Ramboll: CAMx User's Guide, Comprehensive Air Quality model with Extentions, version 7.10, Novato, California, https://www.camx.com/download/source/, (last access: 11 January 2025), 2020.

Ramboll: CAMx v7.10, Ramboll [code], https://www.camx.com/download/source/, last access: 11 January 2025, 2021.

Robinson, A. L., Donahue, N. M., Shrivastava, M. K., Weitkamp, E. A., Sage, A. M., Grieshop, A. P., Lane, T. E., Pierce, J. R., and Pandis, S. N.: Rethinking Organic Aerosols: Semivolatile Emissions and Photochemical Aging, Science, 315, 1259–1262, https://doi.org/10.1126/science.1133061, 2007.

Sandrini, S., van Pinxteren, D., Giulianelli, L., Herrmann, H., Poulain, L., Facchini, M. C., Gilardoni, S., Rinaldi, M., Paglione, M., Turpin, B. J., Pollini, F., Bucci, S., Zanca, N., and Decesari, S.: Size-resolved aerosol composition at an urban and a rural site in the Po Valley in summertime: implications for secondary aerosol formation, Atmospheric Chemistry and Physics, 16, 10 879–10 897, https://doi.org/10.5194/acp-16-10879-2016, 2016.

Schell, B., Ackermann, I., Hass, H., Binkowski, F., and Ebel, A.: Modeling the formation of secondary organic aerosol within a comprehensive air quality model system, Journal of Geophysical Research-Atmospheres, pp. 28 275–28 293, https://doi.org/10.1029/2001JD000384, 2001.

Seibert, R., Nikolova, I., Volná, V., Krejčí, B., and Hladký, D.: Air Pollution Sources' Contribution to PM2.5 Concentration in the Northeastern Part of the Czech Republic, Atmosphere, 11, https://doi.org/10.3390/atmos11050522, 2020.

Seibert, R., Nikolova, I., Volná, V., Krejčí, B., and Hladký, D.: Source Apportionment of PM2.5, PAH and Arsenic Air Pollution in Central Bohemia, Environments, 8, https://doi.org/10.3390/environments8100107, 2021.

https://doi.org/10.5194/egusphere-2025-167
Preprint. Discussion started: 25 April 2025

Shrivastava, M., Fast, J., Easter, R., Gustafson Jr., W. I., Zaveri, R. A., Jimenez, J. L., Saide, P., and Hodzic, A.: Modeling organic aerosols in a megacity: comparison of simple and complex representations of the volatility basis set approach, Atmospheric Chemistry and Physics, 11, 6639–6662, https://doi.org/10.5194/acp-11-6639-2011, 2011.

Singh, A. and Dey, S.: Influence of aerosol composition on visibility in megacity Delhi, Atmospheric Environment, 62, 367–373, https://doi.org/10.1016/j.atmosenv.2012.08.048, 2012.

Skamarock, W. C., Klemp, J. B., Dudhia, J., Gill, D. O., Liu, Z., Berner, J., Wang, W., Powers, J. G., Duda, M. G., Barker, D., and Huang, X.: A Description of the Advanced Research WRF Version 4, NCAR Tech. Note NCAR/TN-556+STR, http://dx.doi.org/10.5065/1dfh-6p97, last access: 25 September 2024, 2019.

Strader, R., Lurmann, F., and Pandis, S. N.: Evaluation of secondary organic aerosol formation in winter, Atmospheric Environment, 33, 4849–4863, https://doi.org/10.1016/S1352-2310(99)00310-6, 1999.

Tsimpidi, A. P., Karydis, V. A., Zavala, M., Lei, W., Molina, L., Ulbrich, I. M., Jimenez, J. L., and Pandis, S. N.: Evaluation of the volatility basis-set approach for the simulation of organic aerosol formation in the Mexico City metropolitan area, Atmospheric Chemistry and Physics, 10, 525–546, https://doi.org/10.5194/acp-10-525-2010, 2010.

Woody, M. C., Baker, K. R., Hayes, P. L., Jimenez, J. L., Koo, B., and Pye, H. O. T.: Understanding sources of organic aerosol during CalNex-2010 using the CMAQ-VBS, Atmospheric Chemistry and Physics, 16, 4081–4100, https://doi.org/10.5194/acp-16-4081-2016, 2016.

WRF: WRF Version 4.2, GitHub [code], https://github.com/wrf-model/WRF/releases, last access: 11 January 2025, 2020.

Wu, T. and Boor, B. E.: Urban aerosol size distributions: a global perspective, Atmospheric Chemistry and Physics, 21, 8883–8914, https://doi.org/10.5194/acp-21-8883-2021, 2021.

Yao, T., Li, Y., Gao, J., Fung, J. C., Wang, S., Li, Y., Chan, C. K., and Lau, A. K.: Source apportionment of secondary organic aerosols in the Pearl River Delta region: Contribution from the oxidation of semi-volatile and intermediate volatility primary organic aerosols, Atmospheric Environment, 222, 117 111, https://doi.org/10.1016/j.atmosenv.2019.117111, 2020.

Zhang, L., Gong, S., Padro, J., and Barrie, L.: A size-segregated particle dry deposition scheme for an atmospheric aerosol module, Atmospheric Environment, 35, 549–560, https://doi.org/10.1016/S1352-2310(00)00326-5, 2001.

Zhang, L., Brook, J. R., and Vet, R.: A revised parameterization for gaseous dry deposition in air-quality models, Atmospheric Chemistry and Physics, 3, 2067–2082, https://doi.org/10.5194/acp-3-2067-2003, 2003.

Zhang, Q., Jimenez, J. L., Canagaratna, M. R., Ulbrich, I. M., Ng, N. L., Worsnop, D. R., and Sun, Y.: Understanding atmospheric organic aerosols via factor analysis of aerosol mass spectrometry: a review, Analytical and Bioanalytical Chemistry, 401, 3045–3067, https://doi.org/10.1007/s00216-011-5355-y, 2011.

Zhang, Y., Huang, H., Qin, W., Yu, Q., Sun, Y., Cheng, S., Ahmad, M., Ouyang, W., Soyol-Erdene, T.-O., and Chen, J.: Modeling of wintertime regional formation of secondary organic aerosols around Beijing: sensitivity analysis and anthropogenic contributions, Carbon Research, 2, https://doi.org/10.1007/s44246-023-00040-w, 2023.

Zhao, Y., Nguyen, N. T., Presto, A. A., Hennigan, C. J., May, A. A., and Robinson, A. L.: Intermediate Volatility Organic Compound Emissions from On-Road Diesel Vehicles: Chemical Composition, Emission Factors, and Estimated Secondary Organic Aerosol Production, Environmental Science & Technology, 49, 11 516–11 526, https://doi.org/10.1021/acs.est.5b02841, 2015.

Zhao, Y., Nguyen, N. T., Presto, A. A., Hennigan, C. J., May, A. A., and Robinson, A. L.: Intermediate Volatility Organic Compound Emissions from On-Road Gasoline Vehicles and Small Off-Road Gasoline Engines, Environmental Science & Technology, 50, 4554–4563, https://doi.org/10.1021/acs.est.5b06247, 2016.